Fluid Phase Equilibria 379 (2014) 26–51

Contents lists available at ScienceDirect

Fluid Phase Equilibria

journal homepage: www.elsevier.com/locate/fluid

A robust algorithm for isenthalpic flash of narrow-boiling fluids

Di Zhu, Ryosuke Okuno*

School of Petroleum Engineering, University of Alberta, Canada

ARTICLE INFO

Article history:
Received 13 February 2014
Received in revised form 1 July 2014
Accepted 3 July 2014
Available online 14 July 2014

Keywords:
Isenthalpic flash
Direct substitution
Equations of state
Narrow-boiling fluids
Bisection

ABSTRACT

Numerical solution of many non-isothermal reservoir flow problems requires robust isenthalpic flash. However, isenthalpic flash is challenging when the total enthalpy is sensitive to temperature, which is referred to as narrow-boiling behavior. The direct substitution (DS) algorithms proposed in the literature have convergence difficulties for narrow-boiling fluids.

This research presents a detailed analysis of the narrow-boiling behavior and its effects on the robustness of the DS algorithms. A new DS algorithm is developed that addresses the direct reason for the convergence issues associated with narrow-boiling behavior. The main focus of the research is on robust isenthalpic flash for two hydrocarbon phases, although mathematical derivations are given for a general multicomponent multiphase system. The thermodynamic model used is the Peng–Robinson equation of state.

The new DS algorithm is tested for various isenthalpic flash problems, which include the cases for which the prior DS algorithms exhibit non-convergence. Results show that the narrow-boiling behavior causes the system of equations solved in the DS algorithms to be degenerate. The degenerate equations can be robustly handled by the bisection algorithm developed in this research. Case studies demonstrate that the new DS algorithm exhibits significantly improved robustness for isenthalpic flash of narrow-boiling fluids.

1. Introduction

Steam injection is a widely used method for heavy-oil recovery [1]. The steam injected releases the latent heat when it condenses into hot water at thermal fronts. Part of the heat can effectively increase the oleic phase mobility because heavy-oil viscosity is highly sensitive to temperature [2,3]. Steam-assisted gravity drainage (SAGD) is an important application of steam injection for recovery of extra-heavy oil and bitumen [4].

Flow of fluid and energy is coupled with multiphase behavior of water–hydrocarbons mixtures in steam injection. A wide variety of compounds that exist in a heavy-oil reservoir have different volatilities. Different compounds propagate differently in a reservoir during the non-isothermal recovery process. Therefore, compositional effects are important in understanding and designing steam injection. For example, thermodynamic conditions at thermal fronts are dependent on multiphase behavior of water–hydrocarbons mixtures at elevated temperatures [5]. Vaporization and condensation of light hydrocarbons, one of the main oil-recovery mechanisms in steam injection, is a consequence of the complex interaction between reservoir flow and multiphase behavior [2,6–10].

Compositional simulation of steam injection has been common practice in the oil industry, in which phase behavior is solved for based on *K*-value tables prepared for different temperatures and pressures [11–13]. The thermal simulation based on *K* values is computationally efficient and reasonably accurate in estimating reservoir processes. However, it does not capture detailed compositional effects on phase equilibria and phase properties. A more general approach to phase behavior modeling is to use a cubic equation of state (EoS) in place of *K*-value tables [9,14–17]. Phase behavior modeling based on an EoS is particularly important when the primary focus of flow simulation is on investigation of detailed recovery mechanisms [9,18]. Recently, Iranshahr et al. [19] presented an efficient EoS thermal simulator on the basis of phase behavior parameterization using tie-line information.

* Corresponding author at: 3-114 Markin/CNRL Natural Resources Engineering Facility, University of Alberta, Edmonton, AB T6G 2W2, Canada. Tel.: +1 780 492 6121; fax: +1 780 492 0249.
E-mail addresses: rokuno@ualberta.ca, okuno@alumni.utexas.net (R. Okuno).

http://dx.doi.org/10.1016/j.fluid.2014.07.003
0378-3812/

Nomenclature

Roman symbols

a	attraction parameter for a cubic equation of state
A	dimensionless attraction parameter for a cubic equation of state
b	covolume parameter for a cubic equation of state
B	dimensionless covolume parameter for a cubic equation of state
C	constant defined for temperature oscillation check
C_{Pj}	heat capacity of phase j
$C_{Pi}{}^0$	coefficients of component i defined in Eq. (17)
$\vec{f}$	vector consisting of N_C residuals of the fugacity equations
f_i	residual of the fugacity equations defined in Eq. (9)
f_{ij}	fugacity of component i in phase j, or residual of the fugacity equations defined in Eq. (5)
f_o	function defined for temperature oscillation check
g_j	residuals of material balance equations ($j = 1, 2, \ldots, N_P - 1$)
g_{N_P}	residual of the enthalpy constraint
$\underline{G}$	molar Gibbs free energy
H	enthalpy
$\underline{H}$	molar enthalpy
k_{ij}	binary interaction parameter between components i and j
$\vec{K}$	vector consisting of N_C K values
K_i	K value of component i for a two-phase system defined in Eq. (10)
K_{ij}	K value of component i in phase j
L	liquid phase
N_C	number of components
N_P	number of phases
P	pressure
P_C	critical pressure
R	universal gas constant
$\underline{S}$	molar entropy
T	temperature
T_C	critical temperature
T_0	273.15 K defined in Eq. (17)
V	vapor phase
$\underline{V}$	molar volume
x_i	mole fraction of component i in the L phase for a L–V two-phase system
x_{ij}	mole fraction of component i in phase j
y_i	mole fraction of component i in the V phase for a L–V two-phase system
z_i	mole fraction of component i in a mixture
Z_j	compressibility factor of phase j

Greek symbols

α	coefficients defined in Eq. (21)
β_j	mole fraction of phase j
ε	convergence criterion (e.g., 10^{-10})
ε_o	constant used for temperature oscillation check
φ_{ij}	fugacity coefficient of component i in phase j
ω	acentric factor

Subscripts

C	critical property
D	dimensionless property
i	component index
j	phase index
m	mixture
ref	reference value
spec	specified value

Superscripts

dep	departure
IG	ideal gas
IGM	ideal gas mixture
k	index for iteration steps
L	lower bound
t	total property

T	transpose
U	upper bound

Abbreviations

BIP	binary interaction parameter
DS	direct substitution
EoS	equation of state
PH	isenthalpic (flash)
PR	Peng–Robinson
PT	isobaric–isothermal (flash)
QNSS	quasi-Newton successive substitution
SAGD	steam-assisted gravity drainage
SS	successive substitution

A common selection of independent variables in EoS thermal simulation is the component mole numbers, pressure, and enthalpy for each grid block [9,17]. Use of enthalpy as an independent variable associated with the energy conservation equation is more general than use of temperature since the former can naturally accommodate the cases of one degree of freedom (e.g., two-component, three-phase systems) [9]. In this simulation formulation, phase behavior at each grid block at each time step is calculated at a given pressure (P), enthalpy (H), and overall composition; i.e., isenthalpic or PH flash.

The most fundamental formulation for PH flash is maximization of entropy (equivalently, minimization of negative entropy) subject to the enthalpy constraint with the variables of temperature and component mole numbers in equilibrium phases [1,9]. Brantferger et al. [9] developed a second-order algorithm for the constrained entropy maximization using Newton's method. The Hessian matrix was modified through the Cholesky decomposition when it was ill-conditioned. However, the non-linearity of the enthalpy constraint made it difficult to ensure robust maximization of the entropy [9,20–23]. Michelsen [22] then proposed another objective function, for which the solution existed at a saddle point of the function. However, it was mentioned that the proposed method could be problematic when narrow-boiling phases were involved [21,22]. The term "narrow-boiling" has been used in the literature to refer to the enthalpy behavior that is very sensitive to temperature [21,24]. Details of the convergence behavior and computational efficiency were not discussed for these function-maximization methods. These methods are quadratically convergent near the solution. It is likely that their robustness depends significantly on initialization of the iteration variables as is the case with minimization of the Gibbs free energy at a given temperature (T) and pressure (P); i.e., PT flash [25–29].

Another type of PH-flash formulation uses PT flash that is nested in the outer temperature iteration loop [24]. This method fundamentally fails for one degree of freedom, where pressure and temperature are interdependent [9,15,24].

Algorithms using Newton's method can be initialized by more robust, but linearly convergent algorithms. In PT flash, for instance, the traditional successive substitution (SS) algorithm and its accelerated variants are commonly used to provide initial estimates for Newton's method [30–35]. A PH-flash algorithm developed by Michelsen [21] had some algorithmic features in common with the SS algorithm for PT flash, and was referred to as the direct substitution (DS) algorithm. In the DS algorithm, the fugacity equations and enthalpy constraint were solved with K values and temperature as independent variables. For each iteration, one Newton's iteration step was performed using the Rachford–Rice equations [36] and the enthalpy constraint as functions of independent phase mole fractions and temperature. Then, K values were updated based on the temperature change that was just obtained by the Newton's iteration step. Unlike the PH flash algorithm using nested PT flash mentioned before, the DS algorithms do not have the issue associated with one degree of freedom since temperature and K values are updated within a single iteration loop [21,24].

The DS algorithm of Michelsen [21] was modified later by Agarwal et al. [24]. The main difference between the DS algorithms of Michelsen and Agarwal et al. was that the latter performed a quasi-Newton update of K values [37,38] prior to the Newton's iteration step for the Rachford–Rice equations and the enthalpy constraint. In general, this preliminary K-value update reduces the number of iterations required for convergence. Siu et al. [39] used the DS algorithm of Agarwal et al. [24] in their fully implicit thermal wellbore model.

Michelsen [21] and Agarwal et al. [24] reported that their DS algorithms could exhibit non-convergence when narrow-boiling phases were involved. The convergence issue was indicated by temperature oscillations in their algorithms, but the reason for the oscillations was not detailed. The suggested remedy was to select the phase compressibility factors in such a way that K values did not converge to unity during the iteration. Although its details were not entirely clear in their papers, it is unlikely that this approach always resolve the convergence issues. For example, there are cases where only a single root exists in solution of a cubic EoS for an oscillating single-phase fluid. More importantly, the direct reason for the convergence issue caused by the presence of narrow-boiling behavior is not the root selection in solution of a cubic EoS as will be presented in Section 3.

Three equilibrium phases consisting of the oleic, gaseous, and aqueous phases are to be handled in application of PH flash in reservoir engineering of thermal oil recovery. However, additional complexities arise when water is part of the fluid system in PH flash; e.g., the model capability of representing the Gibbs free energy that results in mutual solubilities of water and hydrocarbons at a wide temperature–pressure range [40–42], and numerical difficulties associated with extremely small solubilities of hydrocarbons in the aqueous phase [40,41,43–46]. The current paper is focused on the convergence issues associated with narrow-boiling fluids for two hydrocarbon phases, although many mathematical expressions are given for general multicomponent multiphase systems. Robust PH flash for water-containing three-phase systems should consider geometric properties of the Gibbs free energy specific to the thermodynamic model used, and will be presented in future publications.

The main objective of this paper is to develop an improved DS algorithm for two-phase PH flash. First, the formulation and prior DS algorithms for PH flash are discussed. Then, the development begins with detailed analysis of the enthalpy sensitivity to temperature, in which the main contribution of this research lies. The analysis explains the reason for the convergence issues that the prior DS algorithms

can pose for narrow-boiling fluids. The improvement is made to directly address the reason of the convergence issue. Finally, case studies demonstrate the improved robustness of the new DS algorithm.

2. Formulation and conventional algorithms

This section first presents the formulation for PH flash and working equations in the DS algorithm. Then, step-wise descriptions are given for the DS algorithms of Michelsen [21] and Agarwal et al. [24] as implemented in this research.

2.1. Formulation

The most fundamental formulation for PH flash is to maximize the total entropy of a closed system at a specified pressure and enthalpy [1,9]. That is, for a given P, $\underline{H}_{\text{spec}}$ and z_i ($i = 1, 2, \ldots, N_C$), it is to find T and x_{ij} ($i = 1, 2, \ldots, N_C$, and $j = 1, 2, \ldots, N_P$) that maximize

$$\underline{S}^t = \sum_{j=1}^{N_P} \beta_j \underline{S}_j, \tag{1}$$

where $\underline{H}_{\text{spec}}$ is the specified molar enthalpy, z_i is the overall mole fraction of component i, x_{ij} is the mole fraction of component i in phase j, $\underline{S}^t$ is the total molar entropy, β_j is the mole fraction of phase j, $\underline{S}_j$ is the molar entropy of phase j, N_C is the number of components, and N_P is the number of equilibrium phases. The following constraints are to be satisfied:

$$z_i = \sum_{j=1}^{N_P} \beta_j x_{ij} \quad \text{for} \quad i = 1,\ 2,\ \ldots,\ N_C \tag{2}$$

$$\sum_{j=1}^{N_P} \beta_j = 1.0 \tag{3}$$

$$\underline{H}^t = \sum_{j=1}^{N_P} \beta_j \underline{H}_j = \underline{H}_{\text{spec}}, \tag{4}$$

where $\underline{H}^t$ is the total molar enthalpy, and $\underline{H}_j$ is the molar enthalpy of phase j.

Cubic EoSs are widely used in the petroleum industry because of their simplicity, computational efficiency, and reasonable accuracy for representing behavior of petroleum reservoir fluids [47,48]. In this research, the Peng–Robinson (PR) EoS [49,50] is used along with the van der Waals mixing rules [51]. Appendix A presents the PR EoS and thermodynamic derivatives based on the PR EoS that are used in the subsequent sections.

2.2. Direct substitution

The direct substitution (DS) algorithm for PH flash is a root-finding approach, instead of direct maximization of the total entropy. It searches for K values and T that satisfy Eqs. (2)–(4) and the fugacity equations

$$f_{ij} = \ln(x_{ij}\varphi_{ij}) - \ln(x_{iN_P}\varphi_{iN_P}) = 0, \tag{5}$$

where φ_{ij} is the fugacity coefficient of component i in phase j ($i = 1, 2, \ldots, N_C$, and $j = 1, 2, \ldots, N_P - 1$). The K value of component i in phase j is defined as

$$K_{ij} = x_{ij}/x_{iN_P}, \tag{6}$$

where $i = 1, 2, \ldots, N_C$, and $j = 1, 2, \ldots, (N_P - 1)$. The N_Pth phase is the reference phase in Eqs. (5) and (6).

As in the traditional SS algorithm for PT flash, K values are related to β_j and x_{ij} through the Rachford–Rice equations; that is, β_j can be obtained from solution of the Rachford–Rice equations. The Rachford–Rice equations are

$$g_j = \sum_{i=1}^{N_C} \left(x_{ij} - x_{iN_P}\right) = \sum_{i=1}^{N_C} (K_{ij} - 1) z_i / t_i = 0 \quad \text{for} \quad j = 1,\ 2,\ \ldots,\ (N_P - 1), \tag{7}$$

where $t_i = 1 + \sum_{j=1}^{N_P - 1} (K_{ij} - 1)\beta_j$ for $i = 1, 2, \ldots, N_C$ [52]. Then, the corresponding x_{ij} can be obtained from $x_{iN_P} = z_i/t_i$ and Eq. (6) for $j \neq N_P$.

The DS algorithms developed by Michelsen [21] and Agarwal et al. [24] involve solution of the system of N_P equations consisting of Eq. (7) and the enthalpy constraint

$$g_{N_P} = \underline{H}^t - \underline{H}_{\text{spec}} = 0 \tag{8}$$

for T and β_j ($j = 1, 2, \ldots, N_P - 1$) based on Newton's method for root-finding. The Jacobian matrix required is presented in Appendix B for a general N_C-component N_P-phase system. Appendix B also gives the Jacobian matrix for the case of $N_P = 2$, which is the main focus of this paper.

In the conventional two-phase notation for the oleic (L) and gaseous (V) phases, the L phase is the reference phase in Eqs. (5) and (6); thus,

$$f_i = \ln(y_i\varphi_{iV}) - \ln(x_i\varphi_{iL}) = 0, \tag{9}$$

where x_i and y_i are the mole fractions of component i in the L and V phases, respectively. The K value of component i is

$$K_i = y_i/x_i. \tag{10}$$

The Rachford–Rice equation for two phases

$$g_1 = \sum_{i=1}^{N_C}(y_i - x_i) = \sum_{i=1}^{N_C}(K_i - 1)z_i/t_i = 0, \tag{11}$$

where $t_i = 1 + (K_i - 1)\beta_V$ for $i = 1, 2, \ldots, N_C$, and Eq. (8) ($g_2 = 0$) are solved simultaneously for T and β_V. The subsequent subsections present step-wise descriptions of the DS algorithms of Michelsen [21] and Agarwal et al. [24] for $N_P = 2$ (see Appendix B for the 2×2 Jacobian matrix).

2.2.1. Direct substitution algorithm of Michelsen [21]

This subsection presents a step-wise description for the DS algorithm of Michelsen [21].

Step 1. Specify $\underline{H}_{spec}$, P, and z_i, along with model parameters such as critical temperature T_C, critical pressure P_C, acentric factor ω, and $N_C \times N_C$ binary interaction parameters (BIPs).

Step 2. Input an initial guess for temperature, $T^{(1)}$, where the number in the bracket represents the iteration-step number $k = 1$. Calculate initial guesses for K values based on Wilson's correlation [53].

Step 3. Solve Eq. (11) for the vapor phase mole fraction $\beta_V{}^{(k)}$ for the kth iteration step so that $|g_1{}^{(k)}| < \varepsilon_1$ (e.g., $\varepsilon_1 = 10^{-10}$). Calculate the corresponding $x_i{}^{(k)}$ and $y_i{}^{(k)}$.

Step 4. Calculate the residual of the enthalpy constraint ($g_2{}^{(k)}$). If $|g_2{}^{(k)}|$ is less than the tolerance ε_2, stop (e.g., $\varepsilon_2 = 10^{-10}$). Otherwise, continue to step 5.

Step 5. Calculate $\ln \varphi_{ij}{}^{(k)}$, $(\partial \ln \varphi_{ij}/\partial T)^{(k)}$, and phase heat capacities ($C_{Pj}{}^{(k)}$) for j = V and L.

Step 6. Calculate K values using one SS step (i.e., $\ln K_i{}^{(k)} = (\ln \varphi_{iL} - \ln \varphi_{iV})^{(k)}$), $(\partial \ln K_i/\partial T)^{(k)}$, and $g_1{}^{(k)}$.

Step 7. Construct the 2×2 Jacobian matrix (see Appendix B).

Step 8. Perform one Newton's iteration step to obtain $\beta_V{}^{(k+1)}$ and $T^{(k+1)}$.

Step 9. Calculate $f_o = |T^{(k+1)} - T^{(i)}|$, where $i = 1, 2, \ldots, k$, to check for temperature oscillation. Continue to step 10 if f_o is greater than ε_o; $\varepsilon_o = \min_i(|T^{(i)} - T^{(i+1)}|)/C$, where $i = 1, 2, \ldots, (k-1)$ and C (e.g., 10^2) is a constant that defines the investigation radius around $T^{(k+1)}$. Otherwise, temperature is considered to be oscillating. Then, go to step 4 with $\beta_V{}^{(k)} = 0.5$ and $x_i{}^{(k)} = y_i{}^{(k)} = z_i$ only for the first time the oscillation is detected.

Step 10. Update K values; $\ln K_i{}^{(k+1)} = \ln K_i{}^{(k)} + (\partial \ln K_i/\partial \mathrm{T})^{(k)}(T^{(k+1)} - \mathrm{T}^{(k)})$. Go to step 3 after increasing the iteration-step number by one; $k = k + 1$.

The DS algorithm of Michelsen [21] performs one Newton's iteration step to obtain β_V and T in step 8; however, note that its convergence behavior is linear as can be seen in the K-value updates in composition (step 6) and T (step 10). Also, the only stopping criterion is that $|g_2|$ be less than ε_2 in step 4. The other residual for g_1 has been satisfied in step 3. These are also true for the DS algorithm of Agarwal et al. [24] in Section 2.2.2.

In step 5, phase compressibility factors are selected so that the resulting Gibbs free energy is minimized among the possible root selections [54]. This conventional root selection, however, is not applied when step 9 detects temperature oscillation associated with narrow-boiling behavior. For such a case, Michelsen [21] suggested that the oscillating single-phase system be split into two phases of initially equal amounts and compositions (i.e., $\beta_V = 0.5$ and $x_i = y_i = z_i$) only for the first time the oscillation is detected. Then, the maximum compressibility factor is chosen for the V phase and the minimum for the L phase for this iteration step and also the subsequent iterations. However, this scheme does not always resolve the temperature oscillation issue as will be presented in Sections 3 and 5.

How to detect temperature oscillations was not explained in Michelsen [21] and Agarwal et al. [24]. In our implementation of their DS algorithms, it has been observed that the temperature oscillations occur between two distinct temperature ranges in a quite regular manner as will be presented in Sections 3 and 5. Based on the observation, temperature oscillations are detected using the procedure given in step 9. The definition of temperature oscillation becomes stricter if a greater value is used for the C constant.

2.2.2. Direct substitution algorithm of Agarwal et al. [24]

The main modification of the DS algorithm made by Agarwal et al. [24] was that a quasi-Newton step was used for a preliminary update of K values before constructing the Jacobian matrix. The quasi-Newton step used was based on Nghiem [37] and Nghiem and Li [38], and referred to as QNSS. Steps 1–4 are not presented below as they are the same as in Section 2.2.1.

Step 5. Calculate $\ln \varphi_{ij}{}^{(1)}$ and phase heat capacities ($C_{Pj}{}^{(1)}$) for j = V and L.

Step 6. Calculate the residuals of the fugacity equations ($f_i{}^{(1)}$; see Eq. (9)).

Step 7. $T^{(2)} = T^{(1)} - g_2{}^{(1)}/(\sum_j \beta_j C_{Pj})^{(1)}$.

Step 8. Solve Eq. (11) for the vapor phase mole fraction $\beta_V{}^{(k)}$ for the kth iteration step so that $|g_1{}^{(k)}| < \varepsilon_1$. Calculate the corresponding $x_i{}^{(k)}$ and $y_i{}^{(k)}$.

Step 9. Calculate the residual of the enthalpy constraint ($g_2{}^{(k)}$). If $|g_2{}^{(k)}|$ is less than the tolerance ε_2, stop. Otherwise, continue to step 10.

Step 10. Calculate the residuals of the fugacity equations ($f_i{}^{(k)}$; see Eq. (9)).

Step 11. Perform a QNSS step for intermediate K values, $K_i{}^{(k+0.5)}$;

$$\ln \vec{K}^{(k+0.5)} = \ln \vec{K}^{(k)} + \frac{(\ln \vec{K}^{(k)} - \ln \vec{K}^{(k-1)})^{\mathrm{T}} \vec{f}^{(k-1)}}{(\ln \vec{K}^{(k)} - \ln \vec{K}^{(k-1)})^{T}(\vec{f}^{(k)} - \vec{f}^{(k-1)})} \vec{f}^{(k)}, \tag{12}$$

where $\vec{K}$ and $\vec{f}$ are vectors consisting of N_C K values and N_C residuals of the fugacity equations (Eq. (9)), respectively.

Step 12. Calculate $x_i^{(k+0.5)}$ and $y_i^{(k+0.5)}$ based on $\beta_V^{(k)}$ and $K_i^{(k+0.5)}$.
Step 13. Construct the 2×2 Jacobian matrix based on $x_i^{(k+0.5)}$ and $y_i^{(k+0.5)}$.
Step 14. Perform one Newton's iteration step to obtain $\beta_V^{(k+1)}$ and $T^{(k+1)}$.
Step 15. Calculate $f_o = |T^{(k+1)} - T^{(i)}|$, where $i = 1, 2, \ldots, k$, to check for temperature oscillation. Continue to step 16 if f_o is greater than ε_o; $\varepsilon_o = \min_i(|T^{(i)} - T^{(i+1)}|)/C$, where $i = 1, 2, \ldots, (k-1)$ and C (e.g., 10^2) is a constant that defines the investigation radius around $T^{(k+1)}$. Otherwise, temperature is considered to be oscillating. Then, go to step 9 with $\beta_V^{(k)} = 0.5$ and $x_i^{(k)} = y_i^{(k)} = z_i$ only for the first time the oscillation is detected.
Step 16. Update K values; $\ln K_i^{(k+1)} = \ln K_i^{(k)} + (\partial \ln K_i/\partial T)^{(k)}(T^{(k+1)} - T^{(k)})$. Go to step 8 after increasing the iteration-step number by one; $k = k + 1$.

In steps 5 and 10, phase compressibility factors are selected so that the resulting Gibbs free energy is minimized among the possible root selections [54]. As in Section 2.2.1, this conventional root selection is not used when step 15 detects temperature oscillation. For such a case, the procedure of Michelsen [21] described before is followed. The maximum compressibility factor is chosen for the V phase and the minimum for the L phase in step 10 of the subsequent iterations.

3. Analysis of enthalpy sensitivity to temperature

As explained in Section 1, Michelsen [21] and Agarwal et al. [24] reported that their DS algorithms have convergence difficulties when narrow-boiling behavior is involved. A fluid with the narrow-boiling behavior exhibits a significant sensitivity of enthalpy to temperature [21,24]. This section investigates fundamental reasons for the narrow-boiling behavior and its effects on PH flash using the DS algorithm.

3.1. Analytical expression of the total enthalpy

It is important to use temperature and enthalpy of a dimensionless form in PH flash since their magnitudes can significantly affect the condition number of the Jacobian matrix as will be discussed in Section 4. Thus,

$$T_D = T/T_{ref} \tag{13}$$

$$\underline{H}_{Dj} = \underline{H}_j/\underline{H}_{spec}, \tag{14}$$

where T_D is the dimensionless temperature, and $\underline{H}_{Dj}$ is the dimensionless molar enthalpy of phase j. T_{ref} is some reference value to make temperature better scaled in PH flash. For example, T_{ref} can be a temperature near the original reservoir temperature in thermal oil recovery processes (e.g., 300 K). Note that some of the prior PH-flash algorithms in the literature did not use dimensionless temperature and enthalpy.

The dimensionless total molar enthalpy ($\underline{H}_D{}^t$) of N_P phases is

$$\underline{H}_D^t = \sum_{j=1}^{N_P} \beta_j \underline{H}_{Dj} = \sum_{j=1}^{N_P} \beta_j (\underline{H}_{Dj}^{IGM} + \underline{H}_{Dj}^{dep}). \tag{15}$$

The molar phase enthalpy ($\underline{H}_{Dj}$) can be calculated as the summation of the molar ideal-gas-mixture enthalpy ($\underline{H}_{Dj}^{IGM}$) and the molar enthalpy departure ($\underline{H}_{Dj}^{dep}$). The dimensionless molar enthalpy of phase j as an ideal gas mixture, $\underline{H}_{Dj}^{IGM}$, is

$$\underline{H}_{Dj}^{IGM} = \underline{H}_j^{IGM}/\underline{H}_{spec} = \sum_{i=1}^{N_C} x_{ij} \underline{H}_i^{IG}/\underline{H}_{spec}. \tag{16}$$

$\underline{H}_i^{IG}$ is the molar ideal-gas enthalpy for component i and calculated using the following fourth-order polynomial correlation [1,55,56]:

$$\underline{H}_i^{IG} = C_{P1i}^0(T - T_0) + C_{P2i}^0(T^2 - T_0^2)/2 + C_{P3i}^0(T^3 - T_0^3)/3 + C_{P4i}^0(T^4 - T_0^4)/4, \tag{17}$$

where C_{P1i}^0, C_{P2i}^0, C_{P3i}^0, and C_{P4i}^0 are coefficients for component i, and T_0 is 273.15 K.

The dimensionless molar enthalpy departure for phase j is

$$\underline{H}_{Dj}^{dep} = \left\{ \left[\left(RT^2 \frac{\partial A_{mj}}{\partial T} + RTA_{mj} \right) / 2\sqrt{2} B_{mj} \right] \ln \left[\frac{Z_j + (1+\sqrt{2})B_{mj})}{Z_j + (1-\sqrt{2})B_{mj})} \right] + RT(Z_j - 1) \right\} / \underline{H}_{spec} \tag{18}$$

on the basis of the PR EoS. The expressions for A_{mj}, B_{mj}, Z_j, and $\partial A_{mj}/\partial T$ are given in Appendix A.

Now, the sensitivity of $\underline{H}_D{}^t$ to T_D is analyzed using Eq. (15),

$$\frac{\partial \underline{H}_D^t}{\partial T_D} = \sum_{j=1}^{N_P} \frac{\partial \beta_j}{\partial T_D} \underline{H}_{Dj} + \sum_{j=1}^{N_P} \frac{\partial \underline{H}_{Dj}}{\partial T_D} \beta_j. \tag{19}$$

The partial derivative of $\underline{H}_{Dj}$ with respect to T_D can be calculated as follows:

$$\frac{\partial \underline{H}_{Dj}}{\partial T_D} = \sum_{i=1}^{N_C} \frac{\partial \underline{H}_{Dj}}{\partial \underline{H}_j} \frac{\partial \underline{H}_j}{\partial x_{ij}} \frac{\partial x_{ij}}{\partial \beta_j} \frac{\partial \beta_j}{\partial T} \frac{\partial T}{\partial T_D}, \tag{20}$$

where $\partial \underline{H}_{Dj}/\partial \underline{H}_j = 1/\underline{H}_{spec}$ and $\partial T/\partial T_D = T_{ref}$. Appendix A presents the analytical expressions for $\partial \underline{H}_j/\partial x_{ij}$ and $\partial x_{ij}/\partial \beta_j$, and the final expression of Eq. (19) for a general N_C-component N_P-phase system.

Table 1
Properties for the methane (C_1) and *n*-butane (C_4) mixture used for case 1.

Component	Mole fraction	T_C, K	P_C, bar	ω	${C_{P1}}^0$, J/(mol K)	${C_{P2}}^0$, J/(mol K^2)	${C_{P3}}^0$, J/(mol K^3)	${C_{P4}}^0$, J/(mol K^4)
C_1	0.99	190.60	46.00	0.008	19.250	5.212×10^{-2}	1.197×10^{-5}	-1.132×10^{-8}
C_4	0.01	425.20	38.00	0.193	9.487	3.313×10^{-1}	-1.108×10^{-4}	-2.822×10^{-9}

Binary interaction parameters are all zero.
Critical temperature: 197.57 K.
Critical pressure: 53.05 bar.
Two-phase temperature region at $P = 50.00$ bar: [194.98, 228.20] K.

An important result is obtained for two phases. The partial derivative of ${\underline{H}_D}^t$ with respect to T_D can be rewritten as

$$\frac{\partial \underline{H}_D^t}{\partial T_D} = \alpha_1(T_D)\left(\frac{\partial \beta_V}{\partial T_D}\right)^2 + \alpha_2(T_D)\frac{\partial \beta_V}{\partial T_D} + \alpha_3(T_D), \tag{21}$$

where $\alpha_1(T_D)$, $\alpha_2(T_D)$, and $\alpha_3(T_D)$ are terms dependent on T_D. Appendix A presents the detailed analytical expressions for Eq. (21), including those for α_1, α_2, and α_3. Eq. (21) is useful in analyzing the sensitivity of ${\underline{H}_D}^t$ with respect to T_D based only on the four terms, α_1, α_2, α_3, and $\partial\beta_V/\partial T_D$. Particularly, $\partial\beta_V/\partial T_D$ helps understand the physical meaning of narrow-boiling, where the amount of the V phase (i.e., β_V) rapidly increases with a small change in temperature (T_D). That is, a narrow-boiling system exhibits a large value for $|\partial\beta_V/\partial T_D|$ as will be presented later. Unfortunately, a similar expression of Eq. (20) has not been found for a general N_P-phase system.

3.2. Gibbs free energy analysis

The previous section presents the analytical expression of the sensitivity of ${\underline{H}_D}^t$ to T_D in terms of $\partial\beta_V/\partial T_D$. By definition, however, $\partial\beta_V/\partial T_D$ is zero in the Jacobian matrix in the DS algorithms. This subsection gives another analysis of the narrow-boiling behavior through the Gibbs free energy in composition-temperature space.

Phase equilibrium predictions at T and P are determined by the geometric properties of the single-phase Gibbs free energy (i.e., the Gibbs free energy assuming a single phase even in multiphase regions) in composition space. PT flash calculation, or minimization of the Gibbs free energy, is to correct the non-convex portion of the single-phase Gibbs free energy that contains the specified overall composition. The single-phase Gibbs free energy change on mixing in a dimensionless form ($\Delta_m \underline{G}/RT$) is calculated as

$$\Delta_m \underline{G}/RT = \sum_{i=1}^{N_C} x_i[\ln \varphi_i(T,\ P,\ \underline{x}) - \ln \varphi_i(T,\ P)], \tag{22}$$

where $\varphi_i(T, P, \underline{x})$ is the fugacity coefficient of component i in a mixture, and $\varphi_i(T, P)$ is the fugacity coefficient of component i as a pure component.

If β_V is sensitive to T_D for a fixed overall composition and pressure, the Gibbs free energy should behave in such a way that at least one of the equilibrium phase compositions drastically changes with a small change in temperature. This is illustrated in a simple example (case 1) given below.

Case 1 uses a binary mixture of 99.00% methane (C_1) and 1.00% *n*-butane (C_4), for which properties are given in Table 1. Fig. 1 shows the phase envelope in P–T space, where the critical point is calculated to be 197.57 K and 53.05 bar. The contour lines for β_V in Fig. 1a indicate that the sensitivity of β_V to T varies in the two-phase region. The contour lines are significantly dense near the bubble-point curve. PH flash is challenging near the bubble-point at 50 bar since it presents narrow-boiling behavior and is close to the critical point. Fig. 1b shows the magnified P–T diagram near the critical point. At 50 bar, two phases exist from 194.98 K to 228.20 K, and β_V increases from 0.00 to more than 0.90 with a temperature increase of 2.00 K from the bubble-point temperature 194.98 K. Fig. 2 shows that $\underline{H}^t$ and β_V at 50 bar are sensitive to temperature near the bubble point. The $\partial\beta_V/\partial T_D$ can be higher than 70, where T_D is calculated using Eq. (13) with $T_{ref} = 300$ K.

Fig. 3 presents the Gibbs free energy surfaces (Eq. (22)) in composition space at two different temperatures, $T_1 = 195.00$ K and $T_2 = 201.00$ K, at 50.00 bar. As can be seen from Fig. 1, T_1 and T_2 are in the two-phase region, but T_1 is close to the bubble-point temperature. In Fig. 3, equilibrium phases are indicated as follows: the filled circle for the V phase at T_1, the hollow circle for the V phase at T_2, the filled square for the L phase at T_1, and the hollow square for the L phase at T_2. At T_1, the two phases are present near the C_1 edge in composition space. Details of the Gibbs free energy surfaces near the C_1 edge are shown in Fig. 3b.

As temperature increases from T_1 to T_2 ($T_2 - T_1 = 6.00$ K), the composition and the Gibbs free energy of the L phase drastically change. However, this does not occur for the V phase. At T_1, the total $\Delta_m \underline{G}/RT$ is -2.065×10^{-2}, where the C_1 concentration is 98.96% for the L phase and 99.61% for the V phase. The Gibbs free energy values are -2.141×10^{-2} for the L phase and -9.549×10^{-3} for the V phase. At T_2, the total $\Delta_m \underline{G}/RT$ is -1.435×10^{-2}, where the C_1 concentration is 80.26% for the L phase and 99.64% for the V phase. The Gibbs free energy values are -2.209×10^{-1} for the L phase and -7.280×10^{-3} for the V phase. The L phase composition moves away from the fixed overall composition while the V phase composition changes only slightly. As a result, β_V exhibits a drastic change from 0.0644 at T_1 to 0.9669 at T_2.

Fig. 4 shows the significant non-linearity of the phase compositions with respect to temperature. The derivatives of $\ln x_{C4}$ and $\ln y_{C4}$ with respect to T_D are close to zero for temperatures above 205 K in the two-phase region. However, they rapidly increase as the bubble-point temperature is approached. A similar level of non-linearity is observed for the fugacity coefficients since they are thermodynamic properties dependent on the phase composition.

Case 1 has demonstrated that the sensitivity of a phase composition causes the sensitivity of thermodynamic quantities and their associated parameters (e.g., β_V) to temperature for a fixed pressure and overall composition in a two-phase region. Then, the sensitivity of β_V to temperature causes ${\underline{H}_D}^t$ to be sensitive to temperature as discussed above with Fig. 2. This can be also confirmed using Eq. (21). Fig. 5 shows the values for α_1, α_2, and α_3 in Eq. (21) for case 1 between 194.98 K and 228.20 K. The α_1 values are positive near zero. Therefore, the first term of Eq. (21), which is also positive as shown in Fig. 6, does not adversely affect the sensitivity of ${\underline{H}_D}^t$. Fig. 5 indicates that the second and third terms cause ${\underline{H}_D}^t$ to rapidly increase with temperature near the bubble point. Fig. 6 shows that the three terms exhibit

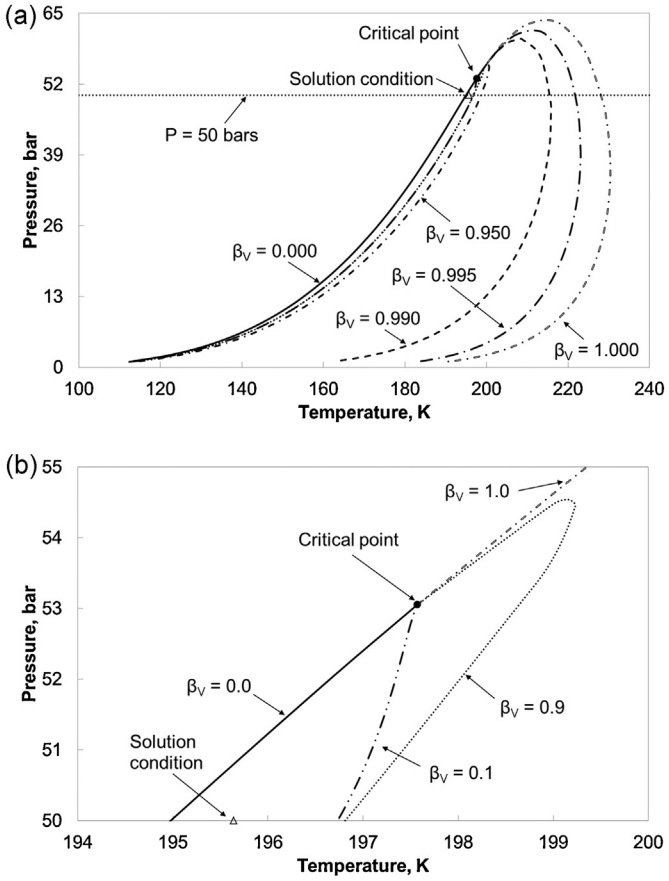

Fig. 1. Two-phase envelope in P–T space for a mixture of 99% C_1 and 1% C_4 (case 1). The properties used for the components are given in Table 1. The critical point is calculated to be 197.57 K and 53.05 bar with the PR EoS. (a) The β_V contour lines are significantly dense near the bubble-point curve. The solution temperature (195.65 K) for an example PH calculation at P = 50 bar and $\underline{H}_{spec}$ = −6500 J/mol exists in the vicinity of the bubble-point curve. (b) Magnified PT diagram near the critical point shows that the solution for the example calculation exists in the region of narrow-boiling behavior.

significant non-linearities with respect to temperature. The large positive values of $\partial\beta_V/\partial T_D$ are multiplied by negative α_2 values for the second term of Eq. (21). The α_3 values are sensitive near the bubble-point temperature, but $\partial\beta_V/\partial T_D$ is not multiplied by α_3 for the third term. The $\partial\beta_V/\partial T_D$ value influences the sensitivity of $\underline{H}_D{}^t$ to temperature mainly through the second term of Eq. (21) in this case.

3.3. Near degeneracy of the system of equations

The previous section showed that the narrow-boiling behavior occurs when at least one of the two phase compositions is sensitive to temperature, causing β_V to be sensitive to temperature. This subsection discusses the effects of narrow-boiling behavior on the condition number of the Jacobian matrix in the DS algorithms, which significantly affects the computational robustness.

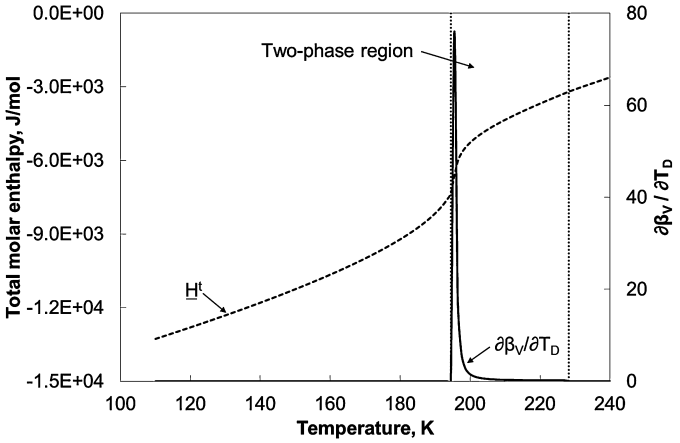

Fig. 2. The total molar enthalpy and the sensitivity of β_V to temperature at 50 bar for a mixture of 99% C_1 and 1% C_4 (case 1). The properties used for the components are given in Table 1. Two phases are present from 194.98 K to 228.20 K. The total molar enthalpy and β_V at 50 bar are sensitive to temperature near the bubble point. The $\partial\beta_V/\partial T_D$ can be higher than 70, where T_D is calculated using Eq. (13) with T_{ref} of 300 K.

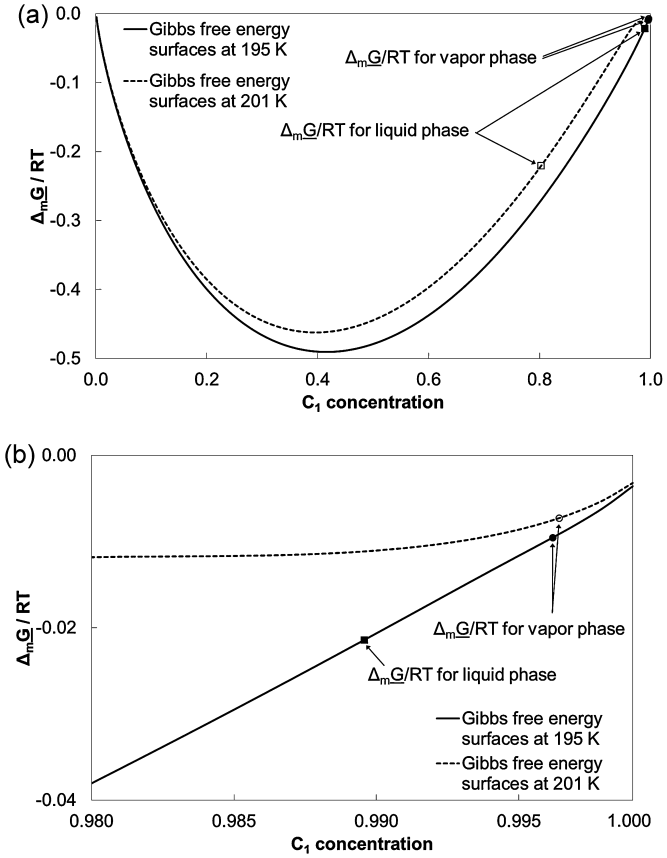

Fig. 3. (a) Gibbs free energy surfaces in binary composition space (case 1) at 50 bar at two different temperatures $T_1 = 195$ K and $T_2 = 201$ K. The properties used for the components are given in Table 1. (b) Magnified Gibbs free energy surfaces near the C_1 edge of composition space. As temperature increases from T_1 to T_2, the L phase composition drastically changes. β_V changes from 0.0644 at T_1 to 0.9669 at T_2.

As presented in Appendix B, the Jacobian matrix for the DS algorithm contains $\partial \ln K_i/\partial T_D$; thus, the behavior of phase compositions affects the condition number of the Jacobian matrix. This is depicted in Fig. 7 for case 1. Fig. 7 shows that $\partial \ln K_{C4}/\partial T_D$ substantially increases with increasing temperature near the bubble-point temperature. This sensitive K_{C4} directly affects the condition number of the Jacobian matrix as shown in Fig. 8. All calculations in this research use the double-precision floating-point numbers, and the Jacobian matrix with a condition number higher than 10^6 is considered to be ill-conditioned. The condition number of the Jacobian matrix is calculated using the one-norm approximation in this research. $\ln K_{C4}$ is significantly sensitive to temperature between 194.98 K and 204.40 K, where the Jacobian matrix is ill-conditioned. That is, narrow-boiling behavior adversely affects the robustness of the DS algorithm through the Jacobian matrix. K values during the DS solution are calculated as the fugacity-coefficient ratio, not from the definition given in Eq. (10), until its convergence. However, the fugacity coefficients are directly related to phase compositions since they are thermodynamic properties dependent on the phase composition. Therefore, the ill-conditioned Jacobian can occur due to sensitive phase compositions during the DS iteration.

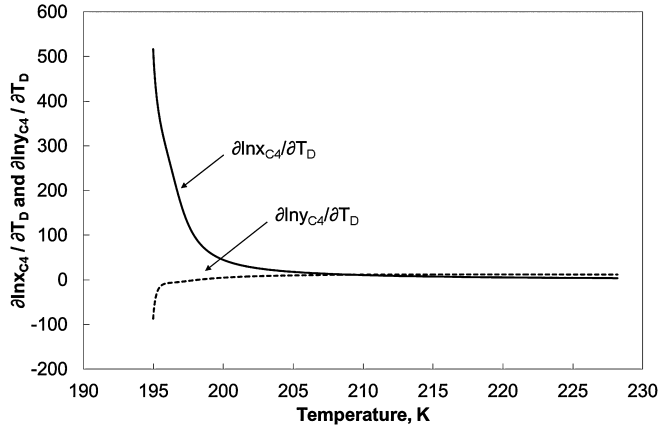

Fig. 4. Sensitivities of the C_4 concentrations in the V and L phases to temperature at 50 bar for a mixture of 99% C_1 and 1% C_4 (case 1). The properties used for the components are given in Table 1.

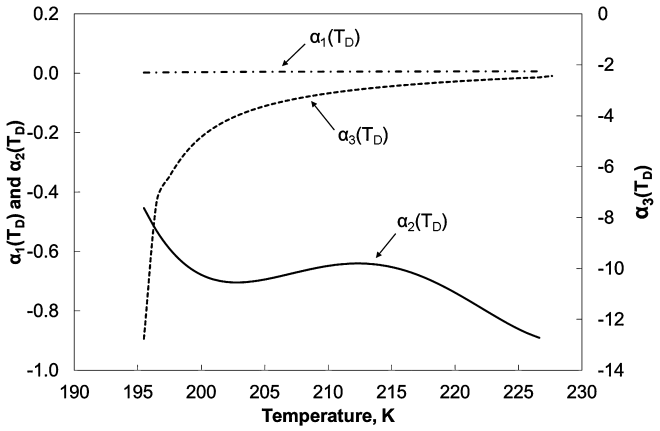

Fig. 5. Three parameters α_1, α_2, and α_3 of Eq. (21) at 50 bar for a mixture of 99% C_1 and 1% C_4 (case 1). The properties used for the components are given in Table 1.

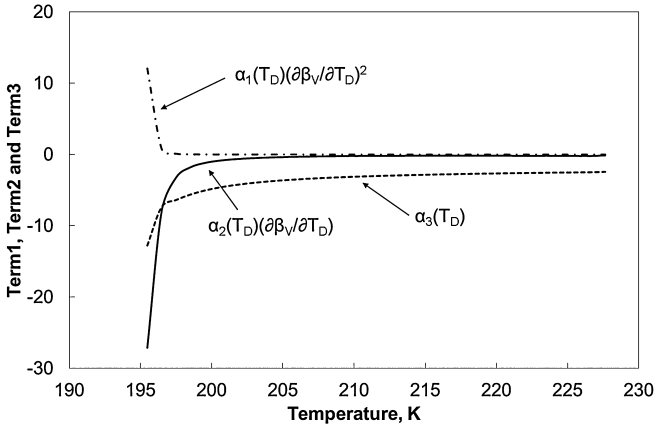

Fig. 6. Three terms of Eq. (21) at 50 bar for a mixture of 99% C_1 and 1% C_4 (case 1). The properties used for the components are given in Table 1.

The Jacobian matrix becomes even more ill-conditioned if the scaling of the total enthalpy and temperature (i.e., Eqs. (13) and (14)) are not conducted. Fig. 8 shows the condition numbers with and without scaling of the variables for case 1. It is observed that the condition number of the Jacobian matrix with the dimensionless variables is systematically lower than that with the dimensional variables. Higham [57] described the importance of scaling Jacobian elements in solution of a system of equations. Castier [58] used scaled independent variables in his isochoric–isoenergetic flash algorithm.

Although Michelsen [21–23] did not fully explain how the narrow-boiling behavior affected the robustness of the DS algorithm, he stated that the non-linearity of the enthalpy constraint in his PH flash algorithm led to a more complex solution procedure. In the DS algorithms of Michelsen [21] and Agarwal et al. [24], strong temperature oscillations during the iteration were used as an indicator for the narrow-boiling behavior. After detecting the temperature oscillations in a certain way, the remedy proposed was to split the oscillating single phase into two phases of initially equal amounts and compositions. As presented in Section 2.2, solutions of a cubic EoS in this

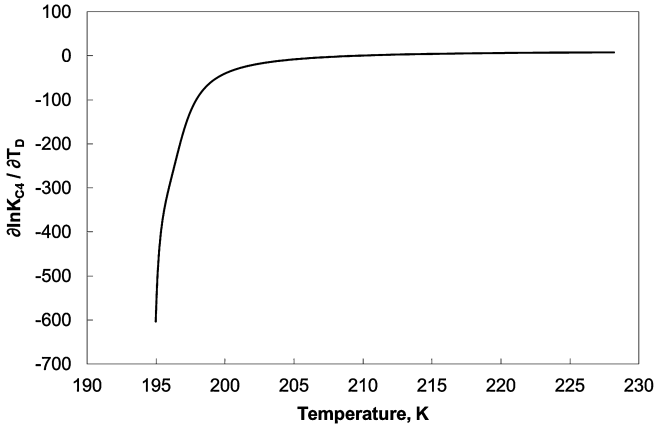

Fig. 7. The first-order derivative of $\ln K_{C4}$ with respect to T_D, showing the sensitivity of K_{C4} to temperature at 50 bar for a mixture of 99% C_1 and 1% C_4 (case 1). The properties used for the components are given in Table 1.

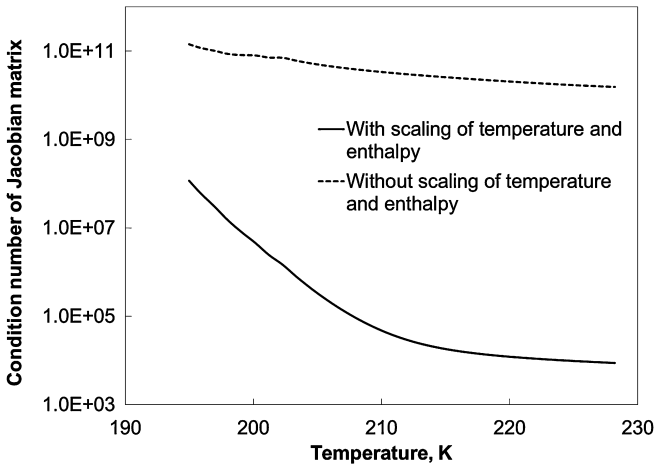

Fig. 8. The condition numbers of the Jacobian matrices with and without scaling of temperature and enthalpy at 50 bar for a mixture of 99% C_1 and 1% C_4 (case 1). The scaling is conducted using Eqs. (13) and (14) with $\underline{H}_{spec}$ of −6500 J/mol and T_{ref} of 300 K. The properties used for the components are given in Table 1.

and the subsequent iteration steps selected the lower compressibility factor for the L phase and the higher for the V phase. They found, however, that this approach did not always improve the non-convergence issues associated with the narrow-boiling behavior [21,24]. For example, it is not unusual that there exists only one root in solution of a cubic EoS for an oscillating single-phase system. For such a case, K values calculated as the fugacity-coefficient ratio become unity in the next iteration step, yielding a singular Jacobian matrix.

The convergence behavior of the prior DS algorithms explained in Section 2.2 is shown for case 1 at 50 bar and $\underline{H}_{spec}$ of −6500 J/mol. The solution temperature is 195.65 K, which is close to the bubble-point temperature in the two-phase region (see Fig. 1). That is, the solution exists in the region of the narrow-boiling behavior. The initial temperature value is set to 190.00 K. The oscillation testing procedure presented in Section 2.2 is used with the C constant of 10^2.

Fig. 9 shows the temperature variations during the iterations for the two DS algorithms. The temperature oscillation is identified at the 6th iteration step for the DS algorithm of Agarwal et al. [24]. A similar oscillation is observed for the DS algorithm of Michelsen [21] in Fig. 9, but the oscillation testing procedure with the C value used does not identify it until the 22nd iteration step. Although Michelsen [21] and Agarwal et al. [24] did not explain how to detect temperature oscillation in their papers, this case indicates that efficient and robust identification of a temperature oscillation in their DS algorithms is not an easy task and would require some heuristic approach. The DS algorithm of Agarwal et al. [24] results in a lower level of temperature oscillation than that of Michelsen [21] in this case. This is likely because of the preliminary update of K values in the DS algorithm of Agarwal et al. [24], which is essentially the only difference between the two DS algorithms.

Once a temperature oscillation is identified, the prior DS algorithms take the remedy proposed by Michelsen [21], which was discussed in Section 2.2 and earlier in this subsection (see also Appendix C). Fig. 10 shows the compressibility factor in composition space at the 22nd iteration step for Michelsen's DS algorithm (218.42 K), and at the 6th iteration step for Agarwal et al.'s DS algorithm (202.67 K). It is shown that only one root exists in the cubic equation solution when the temperature oscillations are identified. This results in a singular Jacobian matrix; thus a complete failure of the calculation. Fig. 11 clearly presents the non-convergence of the DS iterations in terms of the enthalpy constraint (i.e., $g_2 = 0$) for case 1.

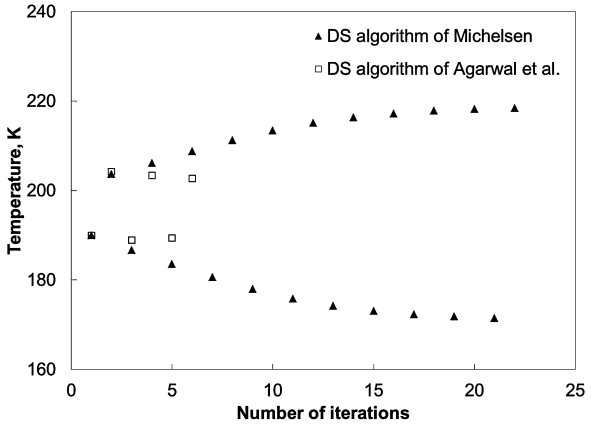

Fig. 9. Convergence behavior of the DS algorithms of Michelsen and Agarwal et al. in terms of temperature in PH flash at $P = 50$ bar and $\underline{H}_{spec} = -6500$ J/mol for a mixture of 99% C_1 and 1% C_4 (case 1). The properties used for the components are given in Table 1. The solution temperature is 195.65 K for this PH calculation. The temperature oscillation is identified at the 6th iteration step for the DS algorithm of Agarwal et al. A similar oscillation is observed for the DS algorithm of Michelsen, but the oscillation testing procedure with the C value used does not identify it until the 22nd iteration step (see Section 2.2 for details of their DS algorithms).

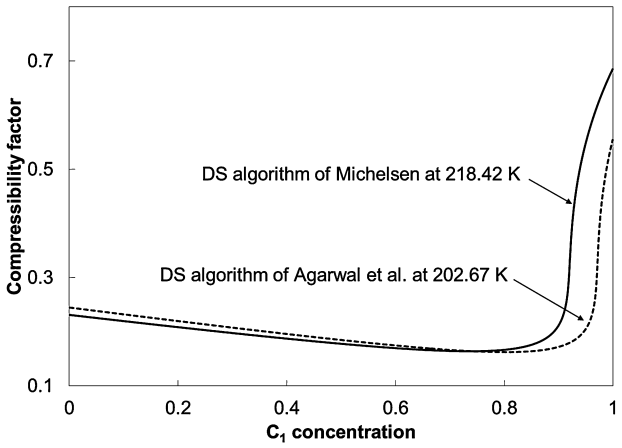

Fig. 10. Compressibility factors in composition space when temperature oscillations are detected during PH flash at $P = 50$ bar and $\underline{H}_{spec} = -6500$ J/mol for a mixture of 99% C_1 and 1% C_4 (case 1). The temperature oscillation occurs at the 22nd iteration step (218.42 K) for Michelsen's DS algorithm, and at the 6th iteration step (202.67 K) for Agarwal et al.'s DS algorithm. In either case, only one compressibility factor is present in the cubic equation solution.

4. New direct substitution algorithm

This section presents a new DS algorithm that improves the issues of the prior DS algorithms associated with the narrow-boiling behavior. There are two main improvements made. One is that the new algorithm checks for the narrow-boiling behavior on the fly on the basis of the condition number of the Jacobian matrix. The condition number contains direct information regarding computational accuracy. A Jacobian matrix with a condition number greater than 10^6 can be safely said to be ill-conditioned when the double-precision floating-point numbers are used [59–61]. Thus, unlike the temperature-oscillation testing used in the prior DS algorithms, the new algorithm has no ambiguity as to how to detect the narrow-boiling behavior. Computation of the condition number for a 2×2 Jacobian matrix is not expensive with the one-norm approximation, and is worth the improved robustness to be presented in Section 5.

The other main improvement is that the new DS algorithm adaptively switches between the Newton's iteration step and bisection step depending on the Jacobian condition number. When a Jacobian matrix is ill-conditioned, the system of equations is essentially degenerate in the computation. Since the degeneracy issue comes from the significant sensitivity of variables to temperature, a robust bisection algorithm solves for T_D as the primary variable. Then, PT flash is used to update other variables such as β_V and K values. This decoupling of T_D from the other variables is performed only if the system of equations is degenerate. Otherwise, the original Newton's iteration step is used.

Other minor improvements made include the use of the upper and lower temperature limits ($T_D{}^U$ and $T_D{}^L$) not to have unrealistic temperature values during the iteration, and the scaling of temperature and enthalpy (i.e., T_D and $\underline{H}_D$). These are not new ideas. The former was applied in the nested-loop algorithm of Agarwal et al. [24] and by Chatoorgoon [62]. The latter is common practice described in standard textbooks in the area of numerical algorithms (e.g., Higham [57] and Overton [63]).

A step-wise description of the new DS algorithm is given below. Steps 1–14 are not shown here since they are the same as in the DS algorithm presented in Section 2.2.2 except for the following: (i) T_D and $\underline{H}_D$ are used in place of T and $\underline{H}$, respectively, and (ii) step 9 also checks to see if the fugacity equations are satisfied in addition to the enthalpy constraint. Appendix C presents a flow chart of the new DS algorithm.

Step 15. Check to see if $T_D{}^L < T_D{}^{(k+1)} < T_D{}^U$. If so, continue to step 16. Otherwise, calculate $T_D{}^{(k+1)}$ using the Regula Falsi method. Then, solve Eq. (11) for the vapor phase mole fraction $\beta_V{}^{(k+1)}$ for the $(k+1)$th iteration step so that $|g_1{}^{(k+1)}| < \varepsilon_1$. Calculate the corresponding $x_i{}^{(k+1)}$ and $y_i{}^{(k+1)}$.

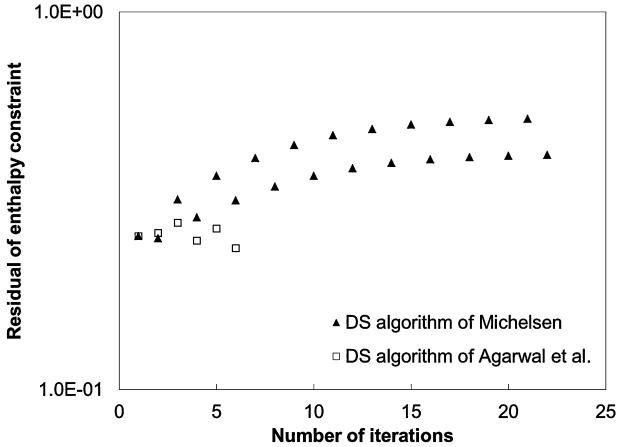

Fig. 11. Convergence behavior of the DS algorithms of Michelsen and Agarwal et al. in terms of the enthalpy constraint in PH flash at $P = 50$ bar and $\underline{H}_{spec} = -6500$ J/mol for a mixture of 99% C_1 and 1% C_4 (case 1). The properties used for the components are given in Table 1.

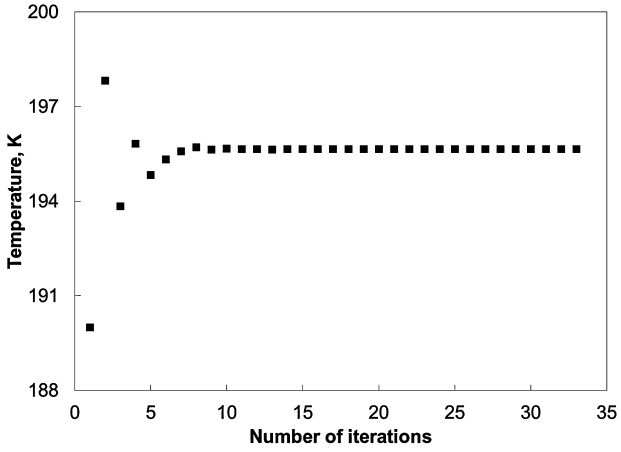

Fig. 12. Convergence behavior of the new DS algorithm in terms of temperature in PH flash at $P = 50$ bar and $\underline{H}_{spec} = -6500$ J/mol for a mixture of 99% C_1 and 1% C_4 (case 1). The properties used for the components are given in Table 1. The solution temperature is 195.65 K for this PH calculation. A high sensitivity of enthalpy to temperature is detected at the 2nd iteration (197.82 K) when the condition number of the Jacobian matrix is 1.68×10^7. The new DS algorithm successfully suppresses the temperature oscillation early in the iterative solution.

Step 16. Calculate the residual of the enthalpy constraint ($g_2^{(k+1)}$) and the fugacity equations (f_i given in Eq. (9)). If $|g_2^{(k+1)}| < \varepsilon_2$ and $|f_i^{(k+1)}| < \varepsilon_f$ (e.g., $\varepsilon_f = 10^{-10}$) for $i = 1, 2, \ldots, N_C$, stop. Otherwise, continue to step 17.

Step 17. Calculate the condition number of the Jacobian matrix. If it is greater than 10^6, go to step 19. Otherwise, continue to step 18.

Step 18. Update K values; $\ln K_i^{(k+1)} = \ln K_i^{(k)} + (\partial \ln K_i / \partial T_D)^{(k)}(T_D^{(k+1)} - T_D^{(k)})$. Go to step 8 after increasing the iteration step number by one; $k = k + 1$.

Step 19-1. $t_L = \min\{T_D^{(k)}, T_D^{(k+1)}\}$ and $t_U = \max\{T_D^{(k)}, T_D^{(k+1)}\}$.

Step 19-2. $T_D^{(k+2)} = 0.5(t_L + t_U)$.

Step 19-3. Perform PT flash at $T_D^{(k+2)}$ to calculate $\beta_V^{(k+2)}$, $x_i^{(k+2)}$, and $y_i^{(k+2)}$ such that $|f_i^{(k+2)}| < \varepsilon_f$ for $i = 1, 2, \ldots, N_C$ and $|g_1^{(k+2)}| < \varepsilon_1$.

Step 19-4. Calculate the condition number of the Jacobian matrix. If it is greater than 10^6, continue to step 19-5. Otherwise, go to step 9.

Step 19-5. Calculate the residual of the enthalpy constraint ($g_2^{(k+2)}$). If $|g_2^{(k+2)}|$ is less than the tolerance ε_2, stop. Otherwise, $t_L = T_D^{(k+2)}$ for $g_2^{(k+2)} < 0$, and $t_U = T_D^{(k+2)}$ for $g_2^{(k+2)} > 0$. Then, go to step 19-2 after increasing the iteration step number by one; $k = k + 1$.

The stopping criterion in the new DS algorithm is that $|g_2| < \varepsilon_2$ and $|f_i| < \varepsilon_f$ for $i = 1, 2, \ldots, N_C$ be satisfied simultaneously. This is in contrast to the prior DS algorithms, where only g_2 is checked [21,24].

5. Case studies

This section shows applications of the new DS algorithm to two mixtures; one is a binary and the other is a six-component mixture. For each mixture, the new DS algorithm is tested for many PH conditions in the two-phase region, part of which exhibits narrow-boiling behavior.

5.1. Case 1

This case was used to explain the narrow-boiling behavior in Section 3. The properties of this binary mixture were presented in Table 1. The prior DS algorithms exhibited non-convergence when applied to this case as shown in Figs. 9 and 11. The specified pressure and enthalpy were 50.00 bar and −6500.00 J/mol, which resulted in the solution temperature of 195.65 K. The initial temperature used was 190.00 K.

In this subsection, the new DS algorithm is used to solve case 1 with $T_{ref} = 300.00$ K, $T^L = 150.00$ K, $T^U = 450.00$ K, and $\varepsilon_1 = \varepsilon_2 = \varepsilon_f = 10^{-10}$. The solution temperature is in the region of the narrow-boiling behavior (see Fig. 1). Newton's iteration step is switched to the bisection algorithm at the second iteration step, when the temperature is 197.82 K and the condition number is 1.68×10^7. The bisection algorithm is used from this iteration step on until the final convergence is achieved at the 33th iteration step. Figs. 12 and 13 present the variations of temperature and g_2 during the iteration. It is observed that the new DS algorithm successfully suppresses the temperature oscillation early in the iterative solution. Unlike the prior DS algorithms, it is not necessary to numerically observe that the temperature oscillates in a regular manner. The bisection algorithm robustly decreases the g_2 residual at a linear convergence rate.

Further testing of the new DS algorithm is performed for 350 discrete points in the two-phase region in the PH diagram given in Fig. 14. The critical point is 53.05 bar and −6794.42 J/mol in this figure. The contour lines are shown for β_V of 0.0, 0.2, 0.5, 0.8, and 1.0. These calculations use the same initial temperature of 190.00 K. The algorithm tends to take more iteration steps for the PH specifications in the region of the narrow-boiling behavior (i.e., the region where the β_V contour lines are dense in Fig. 14). However, all the 350 PH-flash calculations successfully converge to the correct solutions. Fig. 15 presents that the number of iterations required is correlated to the Jacobian condition number at the converged solution. More than 25 iteration steps are required for the PH specifications at which the condition number of the Jacobian matrix is greater than 10^6.

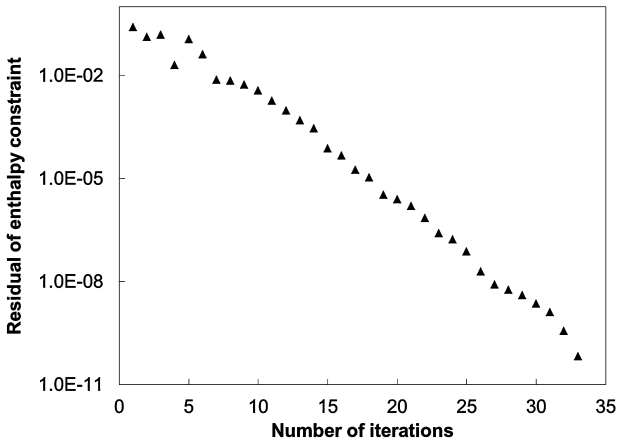

Fig. 13. Convergence behavior of the new DS algorithm in terms of the enthalpy constraint in PH flash at $P = 50$ bar and $\underline{H}_{spec} = -6500$ J/mol for a mixture of 99% C_1 and 1% C_4 (case 1). The properties used for the components are given in Table 1. The new DS algorithm successfully suppresses the temperature oscillation early in the iterative solution. The bisection algorithm robustly decreases the residual for the enthalpy constraint at a linear convergence rate.

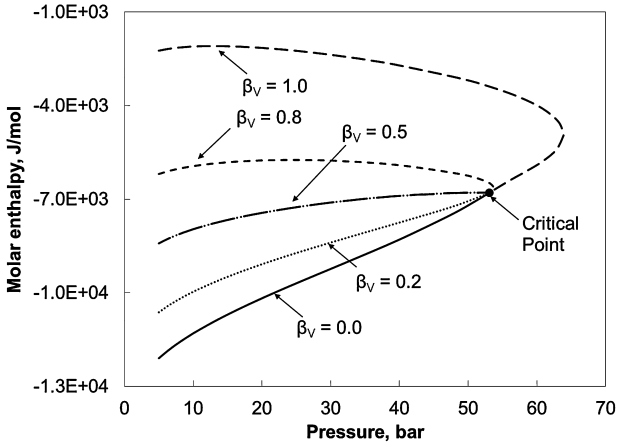

Fig. 14. The two-phase envelope in P–H space for a mixture of 99% C_1 and 1% C_4 (case 1). The properties used for the components are given in Table 1. The critical point is calculated to be 53.05 bar and −6794.42 J/mol with the PR EoS. The contour lines are shown for β_V of 0.0, 0.2, 0.5, 0.8, and 1.0.

5.2. Case 2

Case 2 uses six components consisting of 80.0% carbon dioxide (CO_2), 6.6% methane (C_1), 2.2% propane (C_3), 2.2% *n*-pentane (C_5), 2.2% *n*-octane (C_8), and 6.8% *n*-dodecane (C_{12}). The properties of this mixture are given in Table 2. The critical point is calculated to be 382.58 K and 189.87 bar using the PR EoS. Fig. 16 presents a few contour lines for β_V in P–T space. As in case 1, the contour lines are dense near the bubble-point curve, where a small change in temperature causes a significant change in β_V. Fig. 16b shows a magnified view for pressures between 75 bar and 200 bar and temperatures between 300 K and 390 K.

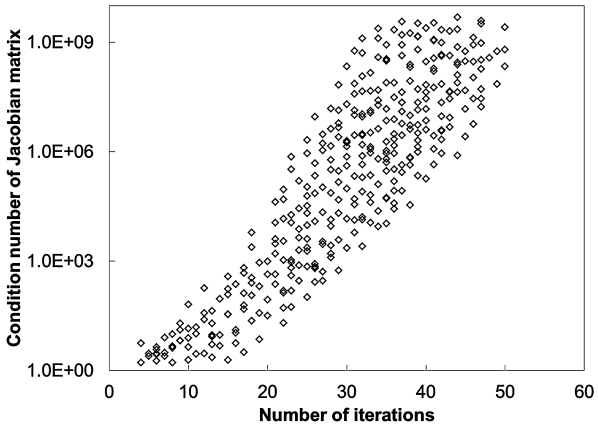

Fig. 15. The number of iterations required for 350 different PH flash calculations in the two-phase region (Fig. 14) is correlated to the condition number of the Jacobian matrix at the converged solution. All the calculations converged to the correct solutions with the new DS algorithm.

Table 2
Properties for the six-component mixture used for case 2.

Component	Mole fraction	T_C, K	P_C, bar	ω	$C_{P1}{}^0$, J/(mol K)	$C_{P2}{}^0$, J/(mol K^2)	$C_{P3}{}^0$, J/(mol K^3)	$C_{P4}{}^0$, J/(mol K^4)
CO_2	0.800	304.20	73.76	0.225	19.795	7.343×10^{-2}	-5.602×10^{-5}	1.715×10^{-8}
C_1	0.066	190.60	46.00	0.008	19.250	5.212×10^{-2}	1.197×10^{-5}	-1.132×10^{-8}
C_3	0.022	369.80	42.46	0.152	−4.224	3.063×10^{-1}	-1.586×10^{-4}	3.215×10^{-8}
C_5	0.022	469.60	33.74	0.251	−3.626	4.873×10^{-1}	-2.580×10^{-4}	5.305×10^{-8}
C_8	0.022	568.80	24.82	0.394	−6.096	7.712×10^{-1}	-4.195×10^{-4}	8.855×10^{-8}
C_{12}	0.068	658.30	18.24	0.562	−9.328	1.149	-6.347×10^{-4}	1.359×10^{-7}

Binary interaction parameters:

	CO_2	C_1	C_3	C_5	C_8	C_{12}
CO_2	0.0000	0.1200	0.1200	0.1200	0.1000	0.1000
C_1	0.1200	0.0000	0.0000	0.0000	0.0496	0.0000
C_3	0.1200	0.0000	0.0000	0.0000	0.0000	0.0000
C_5	0.1200	0.0000	0.0000	0.0000	0.0000	0.0000
C_8	0.1000	0.0496	0.0000	0.0000	0.0000	0.0000
C_{12}	0.1000	0.0000	0.0000	0.0000	0.0000	0.0000

Critical temperature: 382.58 K.
Critical pressure: 189.87 bar.
Two-phase temperature region at P = 77.50 bar: [301.27, 518.79] K.

Fig. 17 shows $\underline{H}^t$ and $\partial\beta_V/\partial T_D$ from 250 K to 550 K at 77.50 bar. The temperature is scaled using Eq. (13) with T_{ref} of 300 K. Two phases are present between 301.27 K and 518.79 K at this pressure. The sensitivities of $\underline{H}^t$ and β_V are observed near the bubble-point temperature. The three terms of Eq. (21) that form $\partial\underline{H}_D{}^t/\partial T_D$ in the two-phase region at 77.50 bar were calculated for case 2. Results showed that, as in case 1, the second term exhibits the most significant non-linearity in temperature space, and drastically increases with a small change in temperature near the bubble point.

The concentrations of components in the L and V phases are sensitive to temperature from the bubble point to 325 K. The condition number of the Jacobian matrix of the DS algorithm becomes significantly large in this temperature range. Fig. 18 shows the Jacobian condition numbers with and without scaling of the variables in the two-phase region at 77.50 bar for case 2. The scaling of temperature

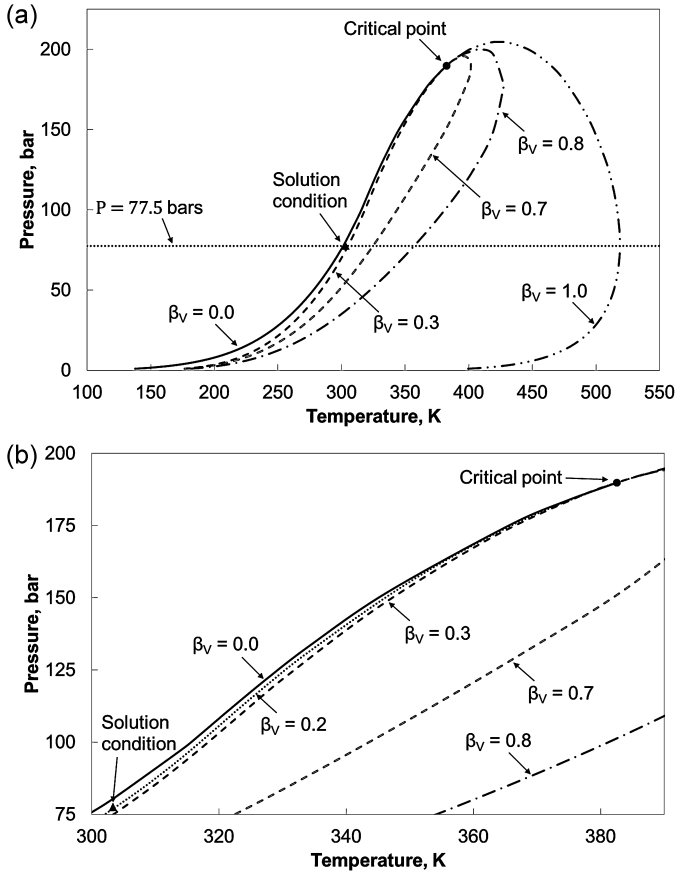

Fig. 16. Two-phase envelope in P–T space for the six-component mixture given in Table 2 (case 2). The critical point is calculated to be 382.58 K and 189.87 bar with the PR EoS. (a) The β_V contour lines are significantly dense near the bubble-point curve. The solution temperature (303.35 K) for an example PH calculation at P = 77.50 bar and $\underline{H}_{spec}$ = −11,000 J/mol exists in the vicinity of the bubble-point curve. (b) PT diagram for pressures between 75 bar and 200 bar and temperatures between 300 K and 390 K. The solution for the example calculation exists in the region of narrow-boiling behavior.

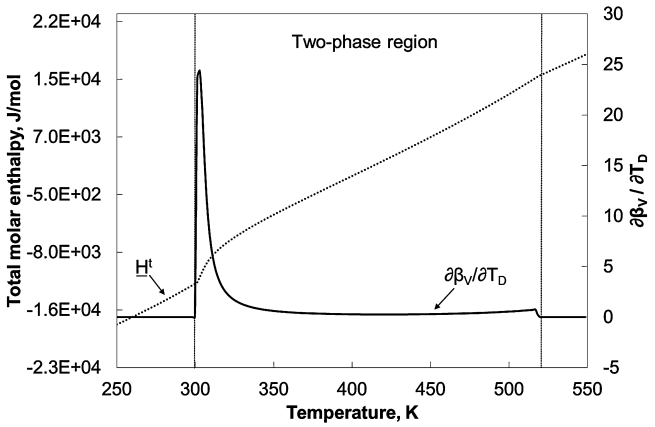

Fig. 17. The total molar enthalpy and the sensitivity of β_V to temperature at 77.50 bar for the six-component mixture given in Table 2 (case 2). Two phases are present from 301.27 K to 518.79 K. $\underline{H}^t$ and β_V are sensitive to temperature near the bubble point temperature at 77.50 bar.

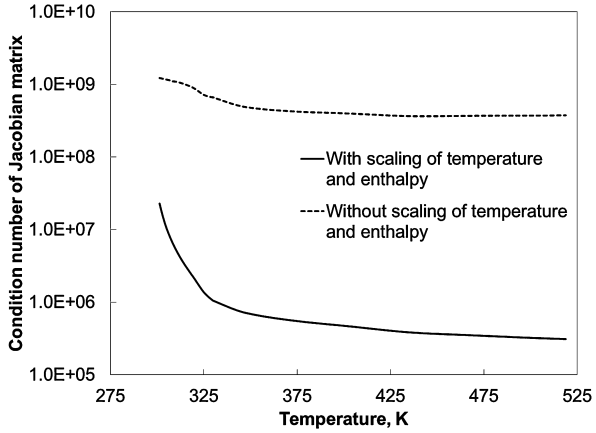

Fig. 18. The condition numbers of the Jacobian matrices with and without scaling of temperature and enthalpy at 77.50 bar for the six-component mixture given in Table 2 (case 2). The scaling is conducted using Eqs. (13) and (14) with $\underline{H}_{spec}$ of −11,000 J/mol and T_{ref} of 300 K. The Jacobian matrix is ill-conditioned in the entire two-phase region without scaling.

and enthalpy is conducted using Eq. (13) and (14) with T_{ref} of 300 K and $\underline{H}_{spec}$ of −11,000 J/mol. Without scaling, the Jacobian matrix is ill-conditioned in the entire two-phase region.

A PH flash calculation at 77.50 bar and −11,000 J/mol is considered for this six-component fluid. The solution temperature is 303.35 K. The initial temperature is set to 425.00 K. Fig. 19 shows the variations of the residual of the enthalpy constraint ($|g_2|$) for the DS algorithms of Michelsen [21] and Agarwal et al. [24]. The temperature oscillation is identified using the approach described in Section 2 with the C constant of 10^2. The temperature oscillation is identified at the fifth iteration (308.63 K) using Michelsen's algorithm, and at the fourth

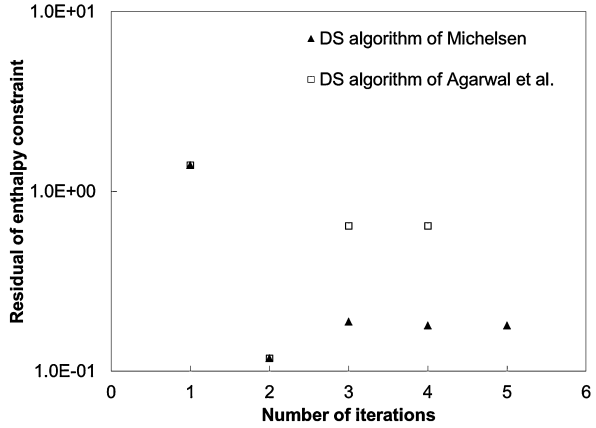

Fig. 19. Convergence behavior of the DS algorithms of Michelsen and Agarwal et al. in terms of the enthalpy constraint in PH flash at 77.50 bar and $\underline{H}_{spec}$ = −11,000 J/mol for the six-component mixture given in Table 2 (case 2). The temperature oscillation is identified at the 5th iteration (308.63 K) using Michelsen's algorithm, and at 4th iteration (342.55 K) using Agarwal et al.'s algorithm. The temperatures are still away from the solution temperature 303.35 K. The two algorithms terminate their calculation here since there is only one root in solution of a cubic EoS.

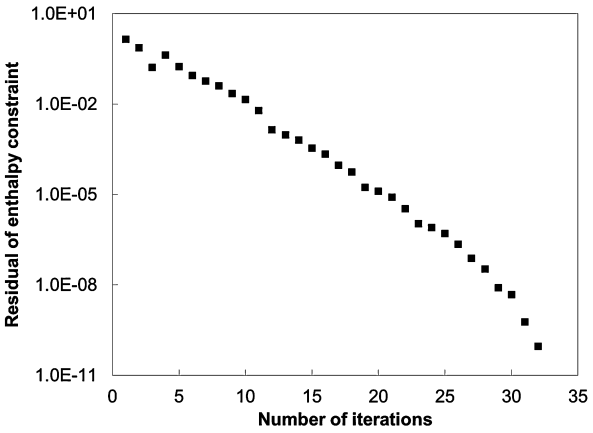

Fig. 20. Convergence behavior of the new DS algorithm in terms of the enthalpy constraint in PH flash at 77.50 bar and $\underline{H}_{spec} = -11{,}000$ J/mol for the six-component mixture given in Table 2 (case 2). The Jacobian condition number exceeds 10^6 at the 4th iteration step, where the bisection algorithm robustly solves for T_D based solely on the enthalpy constraint.

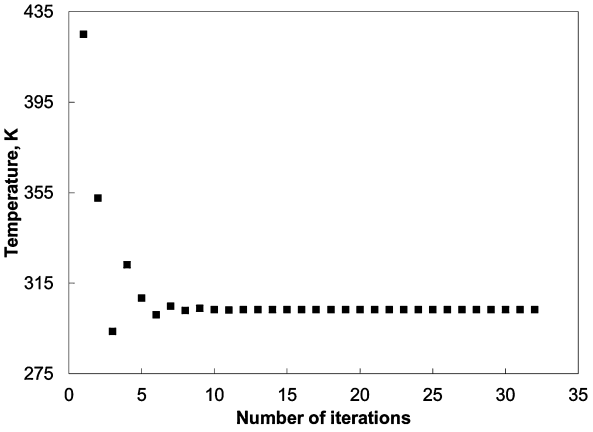

Fig. 21. Convergence behavior of the new DS algorithm in terms of temperature in PH flash at 77.50 bar and $\underline{H}_{spec} = -11{,}000$ J/mol for the six-component mixture given in Table 2 (case 2). The solution temperature is 303.35 K for this PH calculation. A high sensitivity of enthalpy to temperature is detected at the 4th iteration when the condition number of the Jacobian matrix exceeds 10^6.

iteration (342.55 K) using Agarwal et al.'s algorithm. The temperatures are still away from the solution temperature 303.35 K. The two algorithms terminate their calculation here since there is only one root in solution of the cubic EoS. No procedure was given by Michelsen [21] and Agarwal et al. [24] for such a case. Note that these prior DS algorithms do not use the scaled temperature and enthalpy, and their Jacobian matrix is ill-conditioned as shown in Fig. 18.

The new DS algorithm exhibits an improved convergence behavior for this PH flash problem. T^L and T^U are 150.00 K and 450.00 K, respectively, and $\varepsilon_1 = \varepsilon_2 = \varepsilon_f = 10^{-10}$. Figs. 20 and 21 show the residual of the enthalpy constraint and temperature until the convergence

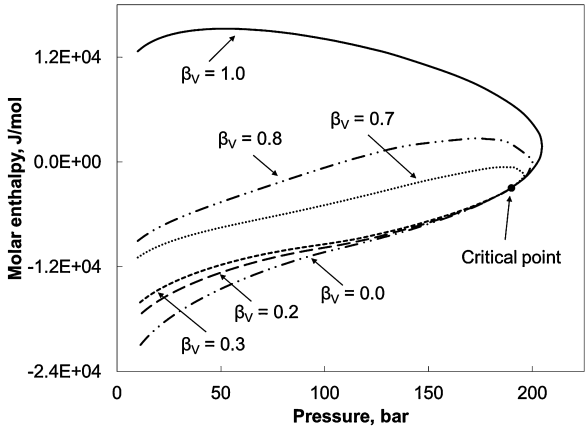

Fig. 22. The two-phase envelope in P-H space for the six-component mixture given in Table 2 (case 2). The critical point is calculated to be 189.87 bar and −2947.69 J/mol with the PR EoS. The contour lines are dense near the bubble-point curve.

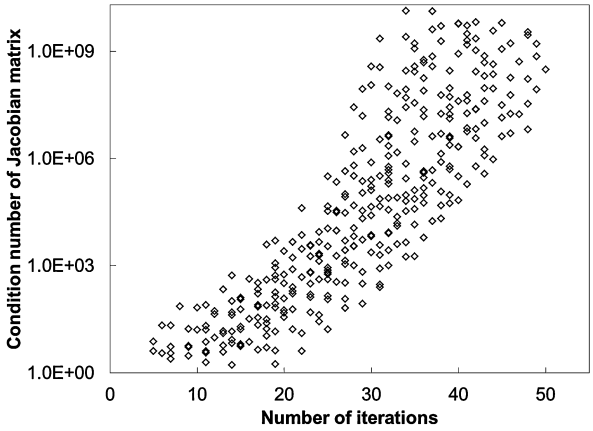

Fig. 23. The number of iterations required for 350 different PH flash calculations in the two-phase region (Fig. 22) is correlated to the condition number of the Jacobian matrix at the converged solution. All the calculations converged to the correct solutions with the new DS algorithm.

is achieved at the 32nd iteration step. The Jacobian condition number exceeds 10^6 from the 4th iteration step on, where the bisection algorithm robustly solves for T_D based solely on the enthalpy constraint.

Fig. 22 shows the two-phase envelope in P-H space for the six-component fluid. The β_V contour lines are dense near the bubble-point curve, where PH flash calculations are more difficult due to the narrow-boiling behavior. The critical point is 189.87 bar and −2947.69 J/mol in this figure. The new DS algorithm is tested for 350 discrete *P–H* conditions in the two-phase region, where the initial temperature is fixed at 425.00 K. All the calculations successfully converge to the correct solutions. Fig. 23 shows that the number of iterations required is well correlated to the condition number of the Jacobian matrix at the convergence.

6. Conclusions

A detailed analysis was presented for narrow-boiling behavior and its effects on the direct substitution (DS) isenthalpic flash for two phases. A new DS algorithm was then developed based on the analysis. No convergence issue has been observed for two-phase isenthalpic flash using the new DS algorithm. Conclusions are as follows:

1. Narrow-boiling behavior is characterized by the enthalpy behavior that is substantially sensitive to temperature. The total enthalpy for a fixed overall composition and pressure becomes sensitive to temperature when at least one of the phase compositions drastically changes with a small change in temperature so that the phase mole fractions significantly change. The mechanistic understanding of the narrow-boiling behavior was presented using the Gibbs free energy surfaces in binary composition space at different temperatures.
2. The prior DS algorithms have convergence issues when narrow-boiling behavior is involved. The fundamental reason is that the system of equations solved in the algorithms becomes degenerate for narrow-boiling fluids. The prior DS algorithms use temperature oscillation as an indicator for narrow-boiling fluids. However, temperature oscillation in these algorithms is a consequence of, not the reason for, the narrow-boiling behavior. That is, it is not a good indicator that improves the robustness.
3. The Jacobian condition number offers an unambiguous criterion regarding the computational accuracy and robustness in the DS algorithm. Computation of the condition number is inexpensive with the one-norm approximation. It is worth the improved robustness.
4. The new DS algorithm developed in this research adaptively switches between Newton's iteration step and the bisection algorithm depending on the Jacobian condition number. The bisection algorithm solves for temperature based solely on the enthalpy constraint when narrow-boiling behavior is identified by a large condition number of the Jacobian matrix. This decoupling of temperature from the other variables is plausible when the system of equations is degenerate.
5. The scaling of temperature and enthalpy can improve the condition number of the Jacobian matrix in the DS algorithms.
6. The new DS algorithm was tested for a binary and six-component fluid which exhibit narrow-boiling behavior. There was no convergence issue observed for 350 different PH flash calculations for the binary fluid, and 350 different PH flash calculations for the six-component fluid. The number of iterations required tends to increase as the condition number of the Jacobian matrix increases at the converged solution.

Acknowledgments

This research was funded by research grants from the Natural Sciences and Engineering Research Council of Canada (RGPIN 418266) and Japan Petroleum Exploration Co., Ltd. (JAPEX). Di Zhu also received financial support from the China Scholarship Council. Ryosuke Okuno was awarded the SPE Petroleum Engineering Junior Faculty Research Initiation Award. We gratefully acknowledge these supports.

Appendix A. Peng–Robinson equation of state and related derivatives

Appendix A.1. Peng–Robinson equation of state

The Peng–Robinson equation of state (PR EoS) is

$$P = RT/(\underline{V} - b) - a/[\underline{V}(\underline{V} + b) + b(\underline{V} - b)], \tag{A-1}$$

where $a = 0.45724(R^2T_C^2/P_C)\alpha$, $b = 0.07780RT_C/P_C$, $\alpha^{0.5} = 1+\kappa[1-(T/T_C)^{0.5}]$, $\kappa = 0.37464 + 1.54226\omega - 0.26992\omega^2$ for $\omega < 0.49$, $\kappa = 0.379642 + 1.48503\omega - 0.164423\omega^2 + 0.016666\omega^3$ for $\omega \geq 0.49$.

The attraction (a) and covolume (b) parameters in a dimensionless form are $A = aP/(RT)^2$ and $B = bP/RT$.

The van der Waals mixing rules are used for the A and B parameters for a mixture. That is,

$$A_m = \sum_{i=1}^{N_C}\sum_{k=1}^{N_C} x_i x_k A_{ik} \tag{A-2}$$

$$B_m = \sum_{i=1}^{N_C} x_i B_i, \tag{A-3}$$

where $A_{ik} = (A_iA_k)^{0.5}(1-k_{ik})$. k_{ik} is the binary interaction parameter between components i and k.

The fugacity coefficient of component i in phase j is

$$\ln\varphi_{ij} = \frac{B_i}{B_{mj}}(Z_j-1) - \ln(Z_j - B_{mj}) - \frac{A_{mj}}{2\sqrt{2}B_{mj}}\left(\frac{2\sum_{k=1}^{N_C}x_kA_{ik}}{A_{mj}} - \frac{B_i}{B_{mj}}\right)\ln\left[\frac{Z_j+(1+\sqrt{2})B_{mj}}{Z_j+(1-\sqrt{2})B_{mj}}\right]. \tag{A-4}$$

The compressibility factor for phase j, Z_j, is calculated from the EoS;

$$Z_j^3 + (B-1)Z_j^2 + (A-3B^2-2B)Z_j + (B^3+B^2-AB) = 0. \tag{A-5}$$

The derivatives of various parameters in the PR EoS with respect to T_D are given below.

$$\frac{\partial a_i}{\partial T_D} = -0.45724R^2T_{Ci}^{1.5}\kappa_i\{1+\kappa_i[1-(T/T_{Ci})^{0.5}]\}T_{ref}/(P_{Ci}\sqrt{T}) \tag{A-6}$$

$$\frac{\partial a_{mj}}{\partial T_D} = \sum_{i=1}^{N_C}\sum_{k=1}^{N_C} 0.5x_{ij}x_{kj}(a_ia_k)^{-0.5}\left(a_i\frac{\partial a_k}{\partial T} + a_k\frac{\partial a_i}{\partial T}\right)(1-k_{ik})T_{ref} \tag{A-7}$$

$$\frac{\partial A_{mj}}{\partial T_D} = \left[\frac{P}{(RT)^2}\frac{\partial a_{mj}}{\partial T} - 2A_{mj}/T\right]T_{ref} \tag{A-8}$$

$$\frac{\partial B_{mj}}{\partial T_D} = -B_{mj}T_{ref}/T \tag{A-9}$$

$$\frac{\partial Z_j}{\partial T_D} = \frac{(\partial A_{mj}/\partial T)(B_{mj}-Z_j) + (\partial B_{mj}/\partial T)[A_{mj} - 2B_{mj} - 3B_{mj}^2 + 2(3B_{mj}+1)Z_j - Z_j^2]}{3Z_j^2 - 2Z_j(1-B_{mj}) + (A_{mj} - 3B_{mj}^2 - 2B_{mj})}T_{ref} \tag{A-10}$$

$$\frac{\partial^2 a_i}{\partial T_D^2} = -0.45724\left(R^2T_{Ci}^{1.5}\kappa_i/P_{Ci}\right)T_{ref}^2\left[\frac{-\kappa_i\sqrt{T}}{2T_{Ci}^2} - \frac{1+\kappa_i[1-T/T_{Ci})^{0.5}]}{2T^{1.5}}\right] \tag{A-11}$$

$$\begin{aligned}\frac{\partial^2 a_{mj}}{\partial T_D^2} &= T_{ref}^2\sum_{i=1}^{N_C}\sum_{k=1}^{N_C} -x_{ij}x_{kj}(a_ia_k)^{-1.5}\left(a_i\frac{\partial a_k}{\partial T} + a_k\frac{\partial a_i}{\partial T}\right)^2(1-k_{ik}) \\ &\quad + T_{ref}^2\sum_{i=1}^{N_C}\sum_{k=1}^{N_C} 0.5x_{ij}x_{kj}(a_ia_k)^{-0.5}\left(2\frac{\partial a_k}{\partial T}\frac{\partial a_i}{\partial T} + a_i\frac{\partial^2 a_k}{\partial T^2} + a_k\frac{\partial^2 a_i}{\partial T^2}\right)(1-k_{ik})\end{aligned} \tag{A-12}$$

$$\frac{\partial^2 A_{mj}}{\partial T_D^2} = T_{ref}^2\left\{\frac{-2P}{R^2T^3}\frac{\partial a_{mj}}{\partial T} + \frac{P}{(RT)^2}\frac{\partial^2 a_{mj}}{\partial T^2} - \frac{2[T(\partial A_{mj}/\partial T) - A_{mj}]}{T^2}\right\} \tag{A-13}$$

Appendix A.2. Derivatives of enthalpy

The partial derivative of $\underline{H}_j$ with respect to x_{ij} in Eq. (20) is

$$\begin{aligned}\frac{\partial \underline{H}_j}{\partial x_{ij}} &= \frac{1}{2\sqrt{2}B_{mj}^2}\left[\left(RT^2\frac{\partial^2 A_{mj}}{\partial T\partial x_{ij}} + RT\frac{\partial A_{mj}}{\partial x_{ij}}\right)B_{mj} - \left(RT^2\frac{\partial A_{mj}}{\partial T} + RTA_{mj}\right)\frac{\partial B_{mj}}{\partial x_{ij}}\right]\ln\left[\frac{Z_j+(1+\sqrt{2})B_{mj}}{Z_j+(1-\sqrt{2})B_{mj}}\right] \\ &\quad + \left[\left(RT^2\frac{\partial A_{mj}}{\partial T} + RTA_{mj}\right)/B_{mj}\right]\frac{[Z_j(\partial B_{mj}/\partial x_{ij}) - B_{mj}(\partial Z_j/\partial x_{ij})]}{[Z_j+(1+\sqrt{2})B_{mj}][Z_j+(1-\sqrt{2})B_{mj}]} + RT\left(\frac{\partial Z_j}{\partial x_{ij}} - 1\right) + \frac{\partial \underline{H}_j^{IGM}}{\partial x_{ij}},\end{aligned} \tag{A-14}$$

where

$$\frac{\partial B_{mj}}{\partial x_{ij}} = \frac{P}{RT}\frac{\partial b_{mj}}{\partial x_{ij}} = B_i$$

$$\frac{\partial A_{mj}}{\partial x_{ij}} = \frac{P}{(RT)^2}\frac{\partial a_{mj}}{\partial x_{ij}} = \sum_{i=1}^{N_C} 2x_{ij}A_{ik}$$

$$\frac{\partial Z_j}{\partial x_{ij}} = \frac{(\partial A_{mj}/\partial x_{ij})(B_{mj}-Z_j)+(\partial B_{mj}/\partial x_{ij})[A_{mj}-2B_{mj}-3B_{mj}^2+2(3B_{mj}+1)Z_j-Z_j^2]}{3Z_j^2-2Z_j(1-B_{mj})+(A_{mj}-3B_{mj}^2-2B_{mj})}$$

$$\frac{\partial^2 A_{mj}}{\partial T\partial x_{ij}} = \frac{P}{(RT)^2}\frac{\partial^2 a_{mj}}{\partial T\partial x_{ij}} - \frac{2}{T}\frac{\partial A_{mj}}{\partial x_{ij}}$$

$$\frac{\partial^2 a_{mj}}{\partial T\partial x_{ij}} = \sum_{i=1}^{N_C} 2(RT)^2(1-k_{ii})\left[\frac{\partial x_{ij}}{\partial T}A_i + x_{ij}\left(\frac{\partial A_i}{\partial T}+\frac{2}{T}A_i\right)\right]/P.$$

Phase composition x_{ij} is calculated as follows:

$$x_{ij} = K_{ij}z_i/t_i, \tag{A-15}$$

where $t_i = 1+\sum_{j=1}^{N_P-1}\beta_j(K_{ij}-1)$ for $i=1, 2, \ldots, N_C$. The partial derivative of x_{ij} with respect to β_j in Eq. (20) is

$$\frac{\partial x_{ij}}{\partial \beta_j} = -K_{ij}z_i(K_{ij}-1)/t_i^2. \tag{A-16}$$

The partial derivative of x_{ij} with respect to T in Eq. (A-14) is

$$\frac{\partial x_{ij}}{\partial T} = \left\{ z_i\frac{\partial K_{ij}}{\partial T}t_i - z_iK_{ij}\sum_{j=1}^{N_P-1}\left[\frac{\partial \beta_j}{\partial T}(K_{ij}-1)+\beta_j\frac{\partial K_{ij}}{\partial T}\right]\right\}/t_i^2. \tag{A-17}$$

The partial derivative of $\underline{H}_{Dj}$ with respect to T_D can be obtained by substituting Eqs. (A-14) and (A-16) into Eq. (20). Consequently, the sensitivity of $\underline{H}_D{}^t$ to T_D can be expressed as

$$\begin{aligned}
\frac{\partial \underline{H}_D^t}{\partial T_D} &= \sum_{i=1}^{N_C}\sum_{j=1}^{N_P}\ln\left[\frac{Z_j+(1+\sqrt{2})B_{mj}}{Z_j+(1-\sqrt{2})B_{mj}}\right]\frac{K_{ij}z_iRT^2}{2\sqrt{2}B_{mj}t_i^2}\sum_{j=1}^{N_P-1}(K_{ij}-1)\beta_j\left[\sum_{i=1}^{N_C}\frac{2z_iA_i(1-k_{ii})}{t_i^2}\beta_j\frac{\partial K_{ij}}{\partial T}\right]\frac{1}{\underline{H}_{spec}}+\sum_{j=1}^{N_P}\underline{H}_j\frac{T_{ref}}{\underline{H}_{spec}}\frac{\partial \beta_j}{\partial T}\\
&+\sum_{i=1}^{N_C}\sum_{j=1}^{N_P}\ln\left[\frac{Z_j+(1+\sqrt{2})B_{mj}}{Z_j+(1-\sqrt{2})B_{mj}}\right]\frac{-K_{ij}z_iRT^2}{2\sqrt{2}B_{mj}t_i^2}\sum_{j=1}^{N_P-1}(K_{ij}-1)\beta_j\left[\sum_{i=1}^{N_C}\frac{2z_iA_i(1-k_{ii})}{t_i^2}\frac{\partial K_{ij}}{\partial T}\right.\\
&\left.+\sum_{i=1}^{N_C}2x_{ij}(1-k_{ii})\left(\frac{\partial A_i}{\partial T}+\frac{2A_i}{T}\right)\right]\frac{T_{ref}}{\underline{H}_{spec}}\frac{\partial \beta_j}{\partial T}+\sum_{i=1}^{N_C}\sum_{j=1}^{N_P}\ln\left[\frac{Z_j+(1+\sqrt{2})B_{mj}}{Z_j+(1-\sqrt{2})B_{mj}}\right]\frac{-K_{ij}z_iRT}{2\sqrt{2}B_{mj}^2t_i^2}\sum_{j=1}^{N_P-1}(K_{ij}-1)\beta_j\\
&\times\left[B_{mj}\frac{\partial A_{mj}}{\partial x_{ij}}-\left(T\frac{\partial A_{mj}}{\partial T}+A_{mj}\right)\frac{\partial B_{mj}}{\partial x_{ij}}\right]\frac{T_{ref}}{\underline{H}_{spec}}\frac{\partial \beta_j}{\partial T}+\sum_{i=1}^{N_C}\sum_{j=1}^{N_P}\left(T\frac{\partial A_{mj}}{\partial T}+A_{mj}\right)\left(Z_j\frac{\partial B_{mj}}{\partial x_{ij}}-B_{mj}\frac{\partial Z_j}{\partial x_{ij}}\right)\\
&\times\frac{-RTK_{ij}z_i}{t_i^2B_{mj}[Z_j+(1+\sqrt{2})B_{mj}][Z_j+(1-\sqrt{2})B_{mj}]}\sum_{j=1}^{N_P-1}(K_{ij}-1)\beta_j\frac{T_{ref}}{\underline{H}_{spec}}\frac{\partial \beta_j}{\partial T}+\sum_{i=1}^{N_C}\sum_{j=1}^{N_P}\frac{-K_{ij}z_iRT}{t_i^2}\sum_{j=1}^{N_P-1}(K_{ij}-1)\beta_j\\
&\times\left(\frac{\partial Z_j}{\partial x_{ij}}-1\right)\frac{T_{ref}}{\underline{H}_{spec}}\frac{\partial \beta_j}{\partial T}+\sum_{i=1}^{N_C}\sum_{j=1}^{N_P}\frac{-K_{ij}z_i\underline{H}_i^{IG}}{t_i^2}\sum_{j=1}^{N_P-1}(K_{ij}-1)\beta_j\frac{T_{ref}}{\underline{H}_{spec}}\frac{\partial \beta_j}{\partial T}+\sum_{i=1}^{N_C}\sum_{j=1}^{N_P}\ln\left[\frac{Z_j+(1+\sqrt{2})B_{mj}}{Z_j+(1-\sqrt{2})B_{mj}}\right]\\
&\times\frac{K_{ij}z_iRT^2}{2\sqrt{2}B_{mj}t_i^2}\sum_{j=1}^{N_P-1}(K_{ij}-1)\beta_j\left[\sum_{i=1}^{N_C}\frac{2z_iA_i(1-k_{ii})}{t_i^2}(K_{ij}-1)\right]\frac{T_{ref}}{\underline{H}_{spec}}\left(\frac{\partial \beta_j}{\partial T}\right)^2.
\end{aligned} \tag{A-18}$$

In the conventional two-phase notation for oleic (L) and gaseous (V) phases, the L phase is the reference phase in Eq. (A-18); thus, for a two-phase system, the sensitivity of $\underline{H}_D{}^t$ to T_D can be expressed as follows:

$$\frac{\partial \underline{H}_D^t}{\partial T_D} = \alpha_1(T_D)\left(\frac{\partial \beta_V}{\partial T_D}\right)^2+\alpha_2(T_D)\left(\frac{\partial \beta_V}{\partial T_D}\right)+\alpha_3(T_D), \tag{A-19}$$

$$\text{where}\quad \alpha_1(T_D) = \sum_{i=1}^{N_C} \ln\left[\frac{Z_V+(1+\sqrt{2})B_{mV}}{Z_V+(1-\sqrt{2})B_{mV}}\right] \frac{RT^2K_iz_i(K_i-1)\beta_V}{2\sqrt{2}B_{mV}t_i^2} \sum_{i=1}^{N_C} \frac{2z_iA_i(1-k_{ii})(K_i-1)}{t_i^2} \frac{T_{ref}}{\underline{H}_{spec}}$$

$$+ \sum_{i=1}^{N_C} \ln\left[\frac{Z_L+(1+\sqrt{2})B_{mL}}{Z_L+(1-\sqrt{2})B_{mL}}\right] \frac{RT^2z_i(K_i-1)\beta_V}{2\sqrt{2}B_{mL}t_i^2} \sum_{i=1}^{N_C} \frac{2z_iA_i(1-k_{ii})(K_i-1)}{t_i^2} \frac{T_{ref}}{\underline{H}_{spec}}$$

$$\alpha_2(T_D) = \underline{H}_V \frac{T_{ref}}{\underline{H}_{spec}} - \underline{H}_L \frac{T_{ref}}{\underline{H}_{spec}} + \sum_{i=1}^{N_C} \ln\left[\frac{Z_V+(1+\sqrt{2})B_{mV}}{Z_V+(1-\sqrt{2})B_{mV}}\right] \frac{-K_iz_iRT^2(K_i-1)\beta_V}{2\sqrt{2}B_{mV}t_i^2}$$

$$\times \left[\sum_{i=1}^{N_C} \frac{2z_iA_i(1-k_{ii})}{t_i} \frac{\partial K_i}{\partial T} + \sum_{i=1}^{N_C} 2y_i(1-k_{ii}) \left(\frac{\partial A_i}{\partial T} + \frac{2A_i}{T}\right)\right] \frac{T_{ref}}{\underline{H}_{spec}} - \sum_{i=1}^{N_C} \ln\left[\frac{Z_L+(1+\sqrt{2})B_{mL}}{Z_L+(1-\sqrt{2})B_{mL}}\right]$$

$$\times \frac{-z_iRT^2(K_i-1)\beta_V}{2\sqrt{2}B_{mL}t_i^2} \sum_{i=1}^{N_C} 2x_i(1-k_{ii}) \left(\frac{\partial A_i}{\partial T} + \frac{2A_i}{T}\right) \frac{T_{ref}}{\underline{H}_{spec}} + \sum_{i=1}^{N_C} \ln\left[\frac{Z_V+(1+\sqrt{2})B_{mV}}{Z_V+(1-\sqrt{2})B_{mV}}\right] \frac{-K_iz_iRT(K_i-1)\beta_V}{2\sqrt{2}B_{mV}^2t_i^2}$$

$$\times \left[B_{mV}\frac{\partial A_{mV}}{\partial y_i} - \left(T\frac{\partial A_{mV}}{\partial T} + A_{mV}\right)\frac{\partial B_{mV}}{\partial y_i}\right] \frac{T_{ref}}{\underline{H}_{spec}} - \sum_{i=1}^{N_C} \ln\left[\frac{Z_L+(1+\sqrt{2})B_{mL}}{Z_L+(1-\sqrt{2})B_{mL}}\right] \frac{-z_iRT(K_i-1)\beta_V}{2\sqrt{2}B_{mL}^2t_i^2}$$

$$\times \left[B_{mL}\frac{\partial A_{mL}}{\partial x_i} - \left(T\frac{\partial A_{mL}}{\partial T} + A_{mL}\right)\frac{\partial B_{mL}}{\partial x_i}\right] \frac{T_{ref}}{\underline{H}_{spec}} + \sum_{i=1}^{N_C} \left(T\frac{\partial A_{mV}}{\partial T} + A_{mV}\right)\left(Z_V\frac{\partial B_{mV}}{\partial y_i} - B_{mV}\frac{\partial Z_V}{\partial y_i}\right)$$

$$\times \frac{-RTK_iz_i(K_i-1)\beta_V}{t_i^2B_{mV}[Z_V+(1+\sqrt{2})B_{mV}][Z_V+(1-\sqrt{2})B_{mV}]} \frac{T_{ref}}{\underline{H}_{spec}} - \sum_{i=1}^{N_C} \left(T\frac{\partial A_{mL}}{\partial T} + A_{mL}\right)\left(Z_L\frac{\partial B_{mL}}{\partial x_i} - B_{mL}\frac{\partial Z_L}{\partial x_i}\right)$$

$$\times \frac{-RTz_i(K_i-1)\beta_V}{t_i^2B_{mL}[Z_L+(1+\sqrt{2})B_{mL}][Z_L+(1-\sqrt{2})B_{mL}]} \frac{T_{ref}}{\underline{H}_{spec}} + \sum_{i=1}^{N_C} \frac{-K_iz_iRT}{t_i^2}(K_i-1)\beta_V\left(\frac{\partial Z_V}{\partial y_i} - 1\right)\frac{T_{ref}}{\underline{H}_{spec}}$$

$$- \sum_{i=1}^{N_C} \frac{-z_iRT}{t_i^2}(K_i-1)\beta_V\left(\frac{\partial Z_L}{\partial x_i} - 1\right)\frac{T_{ref}}{\underline{H}_{spec}} + \sum_{i=1}^{N_C} \frac{-K_iz_i\underline{H}_i^{IG}}{t_i^2}(K_i-1)\beta_V\frac{T_{ref}}{\underline{H}_{spec}} - \sum_{i=1}^{N_C} \frac{-z_i\underline{H}_i^{IG}}{t_i^2}(K_i-1)\beta_V\frac{T_{ref}}{\underline{H}_{spec}}$$

$$\alpha_3(T_D) = \sum_{i=1}^{N_C} \ln\left[\frac{Z_V+(1+\sqrt{2})B_{mV}}{Z_V+(1-\sqrt{2})B_{mV}}\right] \frac{K_iz_iRT^2(K_i-1)\beta_V}{2\sqrt{2}B_{mV}t_i^2} \left[\sum_{i=1}^{N_C} \frac{2z_iA_i(1-k_{ii})}{t_i^2}\beta_V\frac{\partial K_i}{\partial T}\right] \frac{1}{\underline{H}_{spec}}$$

$$+ \sum_{i=1}^{N_C} \ln\left[\frac{Z_L+(1+\sqrt{2})B_{mL}}{Z_L+(1-\sqrt{2})B_{mL}}\right] \frac{z_iRT^2(K_i-1)\beta_V}{2\sqrt{2}B_{mL}t_i^2} \left[\sum_{i=1}^{N_C} \frac{2z_iA_i(1-k_{ii})}{t_i^2}\beta_V\frac{\partial K_i}{\partial T}\right] \frac{1}{\underline{H}_{spec}}.$$

In Eq. (A-19), $t_i = 1 + (K_i - 1)\beta_V$.

Appendix A.3. Derivatives of phase mole fractions

For a N_C-component N_P-phase system, phase mole fractions β_j are obtained from solution of the Rachford–Rice equations;

$$\sum_{i=1}^{N_C} (K_{ij}-1)z_i/t_i = 0 \quad \text{for } j = 1,\ 2,\ \ldots,\ (N_P-1), \tag{A-20}$$

where $t_i = 1 + \sum_{j=1}^{N_P-1}(K_{ij}-1)\beta_j$ for $i = 1, 2, \ldots, N_C$. The partial derivative of β_j with respect to T_D, $(\partial\beta_j/\partial T_D)$, can be calculated as follows:

$$\sum_{i=1}^{N_C}\sum_{m=1}^{N_P-1}(1-K_{ij})z_i(1-K_{im})\frac{\partial\beta_m}{\partial T} = \sum_{i=1}^{N_C}\frac{\partial K_{ij}}{\partial T}z_it_i + \sum_{i=1}^{N_C}\sum_{m=1}^{N_P-1}(1-K_{ij})z_i\frac{\partial K_{im}}{\partial T}\beta_m. \tag{A-21}$$

For a two-phase system, $\partial\beta_V/\partial T_D$ is expressed as

$$\frac{\partial\beta_V}{\partial T_D} = T_{ref}\sum_{i=1}^{N_C} z_i\frac{\partial K_i}{\partial T} \Big/ \sum_{i=1}^{N_C}(1-K_i)^2z_i \tag{A-22}$$

Appendix B. Jacobian matrix

The elements of the Jacobian matrix for a N_C-component N_P-phase system are

$$\frac{\partial g_j}{\partial T_D} = T_{ref}\sum_{i=1}^{N_C}\frac{z_i}{t_i^2}\left[t_i K_{ij}\frac{\partial \ln K_{ij}}{\partial T} - (K_{ij}-1)\sum_{k=1}^{N_P-1}\beta_k K_{ik}\frac{\partial \ln K_{ik}}{\partial T}\right] \quad \text{for } j = 1, 2, \ldots, (N_P-1) \tag{B-1}$$

$$\frac{\partial g_j}{\partial \beta_k} = -\sum_{i=1}^{N_C}\frac{z_i}{t_i^2}(K_{ij}-1)(K_{ik}-1) \quad \text{for } j, k = 1, 2, \ldots, (N_P-1) \tag{B-2}$$

$$\frac{\partial g_{N_P}}{\partial T_D} = T_{ref}\sum_{j=1}^{N_P}\beta_j\left(\sum_{i=1}^{N_C}\frac{\partial x_{ij}}{\partial T}\frac{\underline{H}_i^{IG}}{\underline{H}_{spec}} + \sum_{i=1}^{N_C}\frac{x_{ij}}{\underline{H}_{spec}}\frac{\partial \underline{H}_i^{IG}}{\partial T} + \frac{\partial \underline{H}_{Dj}^{dep}}{\partial T}\right) \tag{B-3}$$

$$\frac{\partial g_{N_P}}{\partial \beta_k} = (\underline{H}_{Dk}^{IGM} + \underline{H}_{Dk}^{dep}) - (\underline{H}_{DN_P}^{IGM} + \underline{H}_{DN_P}^{dep}) \quad \text{for } k = 1, 2, \ldots, (N_P-1), \tag{B-4}$$

where $t_i = 1 + \sum_{j=1}^{N_P-1}(K_{ij}-1)\beta_j$ for $i = 1, 2, \ldots, N_C$. Pertinent derivatives are

$$\frac{\partial \underline{H}_i^{IG}}{\partial T} = C_{P1i}^0 + C_{P2i}^0 T + C_{P3i}^0 T^2 + C_{P4i}^0 T^3 \quad \text{for } i = 1, 2, \ldots, N_C \tag{B-5}$$

$$\frac{\partial \underline{H}_{Dj}^{dep}}{\partial T} = \frac{1}{\underline{H}_{spec}}\left\{\text{Term1}\times \ln\left[\frac{Z_j + (1+\sqrt{2})B_{mj}}{Z_j + (1-\sqrt{2})B_{mj}}\right] + \frac{RT^2\partial A_{mj}/\partial T + RTA_{mj}}{2\sqrt{2}B_{mj}}\times \text{Term2} + R(Z_j-1) + RT\frac{\partial Z_j}{\partial T}\right\}. \tag{B-6}$$

In Eq. (B-6),

$$\text{Term1} = \left[B_{mj}\left(3RT\frac{\partial A_{mj}}{\partial T} + RT^2\frac{\partial^2 A_{mj}}{\partial T^2} + RA_{mj}\right) - \frac{\partial B_{mj}}{\partial T}\left(RT^2\frac{\partial A_{mj}}{\partial T} + RTA_{mj}\right)\right]/(2\sqrt{2}B_{mj}^2) \tag{B-7}$$

$$\text{Term2} = \frac{[\partial Z_j/\partial T + (1+\sqrt{2})\partial B_{mj}/\partial T][Z_j + (1-\sqrt{2})B_{mj}] - [\partial Z_j/\partial T + (1-\sqrt{2})\partial B_{mj}/\partial T][Z_j + (1+\sqrt{2})B_{mj}]}{[Z_j + (1+\sqrt{2})B_{mj}][Z_j + (1-\sqrt{2})B_{mj}]}. \tag{B-8}$$

$\partial A_{mj}/\partial T$, $\partial B_{mj}/\partial T$, $\partial^2 A_{mj}/\partial T^2$, and $\partial Z_j/\partial T$ can be found in Appendix A.

For a two-phase system, Newton's iteration used in the DS algorithms can be written as

$$\begin{pmatrix} \frac{\partial g_1}{\partial \beta_V} & \frac{\partial g_1}{\partial T_D} \\ \frac{\partial g_2}{\partial \beta_V} & \frac{\partial g_2}{\partial T_D} \end{pmatrix}\begin{pmatrix} \Delta\beta_V \\ \Delta T_D \end{pmatrix} = -\begin{pmatrix} g_1 \\ g_2 \end{pmatrix} \tag{B-9}$$

$$\text{where} \quad \frac{\partial g_1}{\partial \beta_V} = -\sum_{i=1}^{N_C}\frac{z_i}{t_i^2}(K_i-1)^2 \tag{B-10}$$

$$\frac{\partial g_1}{\partial T_D} = T_{ref}\sum_{i=1}^{N_C}\frac{z_i}{t_i^2}\left[t_i K_i\frac{\partial \ln K_i}{\partial T} - \beta_V K_i(K_i-1)\frac{\partial \ln K_i}{\partial T}\right] \tag{B-11}$$

$$\frac{\partial g_2}{\partial \beta_V} = (\underline{H}_{DV}^{IGM} + \underline{H}_{DV}^{dep}) - (\underline{H}_{DL}^{IGM} + \underline{H}_{DL}^{dep}) \tag{B-12}$$

$$\frac{\partial g_2}{\partial T_D} = T_{ref}\left[\beta_V\left(\sum_{i=1}^{N_C}\frac{\partial x_{iV}}{\partial T}\frac{\underline{H}_i^{IG}}{\underline{H}_{spec}} + \sum_{i=1}^{N_C}\frac{x_{iV}}{\underline{H}_{spec}}\frac{\partial \underline{H}_i^{IG}}{\partial T} + \frac{\partial \underline{H}_{DV}^{dep}}{\partial T}\right) + \beta_L\left(\sum_{i=1}^{N_C}\frac{\partial x_{iL}}{\partial T}\frac{\underline{H}_i^{IG}}{\underline{H}_{spec}} + \sum_{i=1}^{N_C}\frac{x_{iL}}{\underline{H}_{spec}}\frac{\partial \underline{H}_i^{IG}}{\partial T} + \frac{\partial \underline{H}_{DL}^{dep}}{\partial T}\right)\right] \tag{B-13}$$

In Eqs. (B-10) to (B-13), $t_i = 1 + (K_i - 1)\beta_V$.

Appendix C. Flow charts of direct substitution algorithms

Appendix C.1. Michelsen [21].

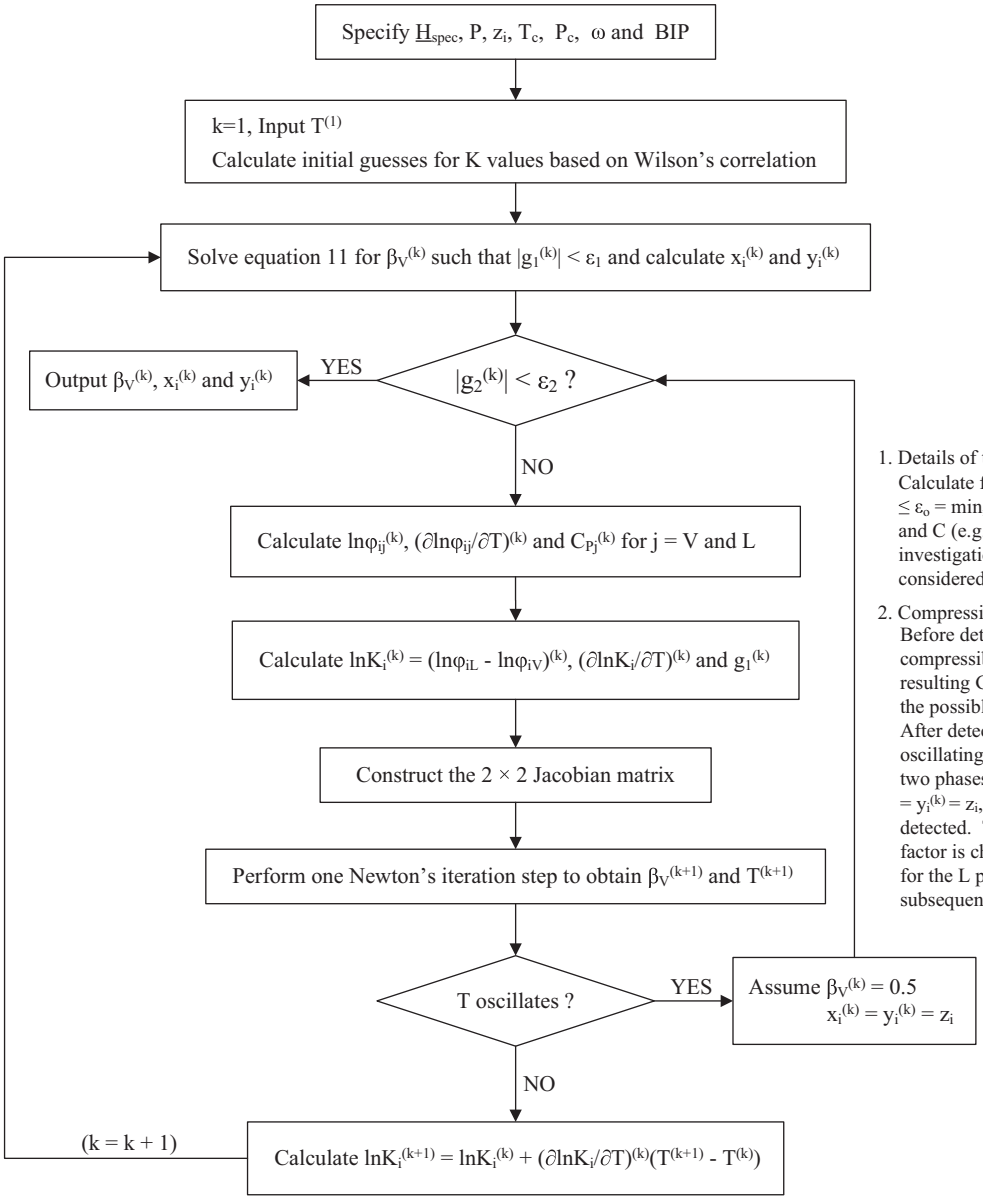

1. Details of the check of temperature oscillation: Calculate $f_o = |T^{(k+1)}\text{-}T^{(i)}|$, where i=1, 2, …, k. If $f_o \le \varepsilon_o = \min_i(|T^{(i)}\text{-}T^{(i+1)}|)/C$, where i=1, 2, …, (k-1) and C (e.g., 10^2) is a constant that defines the investigation radius around $T^{(k+1)}$, temperature is considered to be oscillating.
2. Compressibility factor selection approach: Before detecting temperature oscillation, phase compressibility factors are selected so that the resulting Gibbs free energy is minimized among the possible roots selections. After detecting temperature oscillation, the oscillating single-phase system will be split into two phases with the assumption $\beta_V^{(k)} = 0.5$ and $x_i^{(k)} = y_i^{(k)} = z_i$, only for the first time the oscillation is detected. Then, the maximum compressibility factor is chosen for the V phase and the minimum for the L phase for this iteration step and subsequent iterations.

Appendix C.2. Agarwal et al. [24].

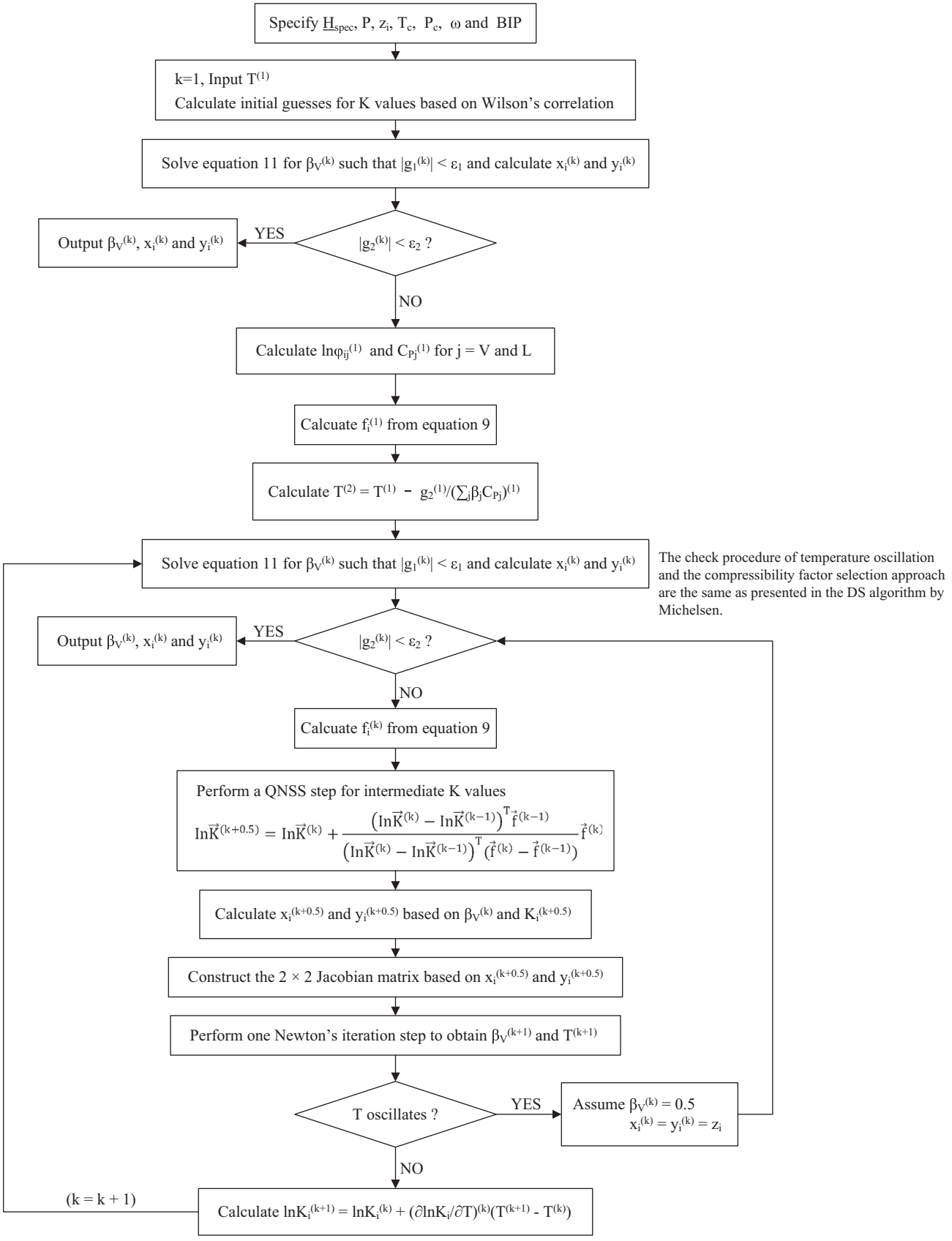

Appendix C.3. New direct substitution algorithm presented in Section 4.

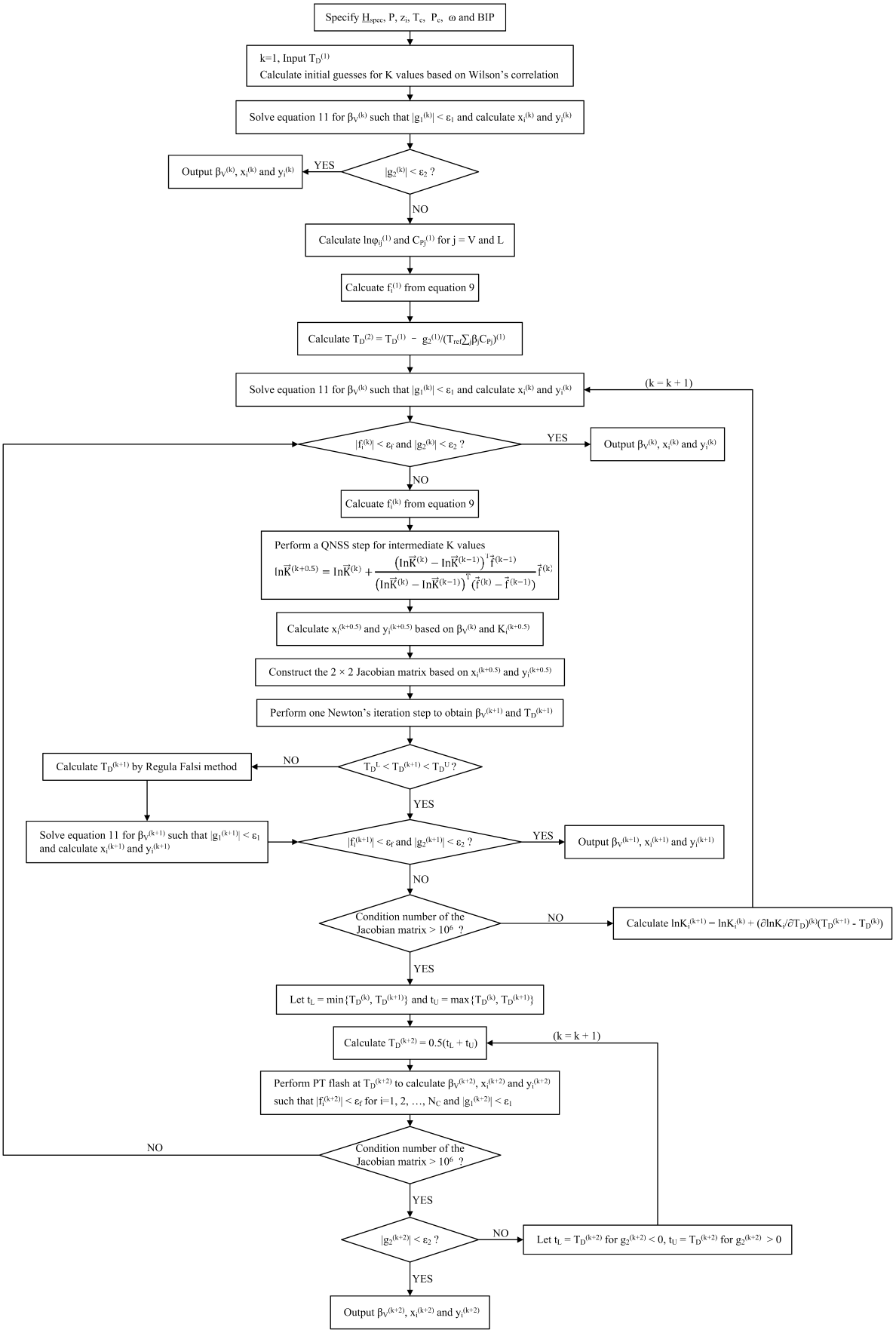

References

[1] K.M. Brantferger, Development of a Thermodynamically Consistent, Fully Implicit, Compositional, Equation-of-State, Steamflood Simulator (PhD dissertation), The University of Texas at Austin, Austin, TX, 1991.
[2] M. Prats, Thermal Recovery, SPE Monograph Series, vol. 7, Dallas, 1982.
[3] A. Varavei, Development of an Equation-of-State Thermal Flooding Simulator (PhD dissertation), The University of Texas at Austin, Austin, TX, 2009.
[4] R.M. Butler, Thermal Recovery of Oil and Bitumen, Prentice Hall, NJ, 1991.
[5] M. Keshavarz, R. Okuno, T. Babadagli, Optimal Application Conditions for Steam-Solvent Coinjection. Paper presented at the SPE Heavy Oil Conference-Canada, June 11–13, Calgary, Alberta, Canada, 2013.
[6] B.T. Willman, V.V. Valleroy, G.W. Runberg, A.J. Cornelius, L.W. Powers, 1537-G-Laboratory studies of oil recovery by steam injection, J. Pet. Technol. 13 (7) (1961) 681–690.
[7] J. Hagoort, A. Leijnse, F. Van Poelgeesi, Steam-strip drive: a potential tertiary recovery process, J. Pet. Technol. 28 (12) (1976) 1409–1419.
[8] W.R. Shu, K.J. Hartman, Effect of solvent on steam recovery of heavy oil, SPE Reserv. Eng. 3 (2) (1988) 457–465.
[9] K.M. Brantferger, G.A. Pope, K. Sepehrnoori, Development of a Thermodynamically Consistent, Fully Implicit, Equation-of-State, Compositional Steamflood Simulator. Paper presented at the SPE Symposium on Reservoir Simulation, February 17–20, Anaheim, California, 1991.
[10] J. Bruining, D. Marchesin, Maximal oil recovery by simultaneous condensation alkane and steam, Phys. Rev. E: Stat. Nonlinear Soft Matter Phys. 75 (3) (2007) 036312-1–036312-16.
[11] Computer Modelling Group (CMG) Ltd., STARS User Manual, Version 2011, Calgary, Alberta, Canada, 2011.
[12] J.W. Grabowski, P.K. Vinsome, R.C. Lin, G.A. Behie, B. Rubin, A Fully Implicit General Purpose Finite-Difference Thermal Model for In Situ Combustion and Steam. Paper presented at the SPE Annual Technical Conference and Exhibition, September 23–26, Las Vegas, Nevada, 1979.
[13] B. Rubin, W.L. Buchanan, A general purpose thermal model, SPE J. 25 (2) (1985) 202–214.
[14] K. Ishimoto, G.A. Pope, K. Sepehrnoori, An equation of state steam simulator, In Situ 11 (1) (1987) 1–37.
[15] M.C.H. Chien, H.E. Yardumian, E.Y. Chung, W.W. Todd, The Formulation of a Thermal Simulation Model in a Vectorized, General Purpose Reservoir Simulator. Paper presented at the SPE Symposium on Reservoir Simulation, February 6–8, Houston, Texas, 1989.
[16] A. Varavei, K. Sepehrnoori, An EOS-Based Compositional Thermal Reservoir Simulator. Paper presented at the SPE Reservoir Simulation Symposium, February 2–4, The Woodlands, Texas, 2009.
[17] K. Liu, G. Subramanian, D.I. Dratler, J.P. Lebel, J.A. Yerian, A general unstructured-grid, equation-of-state-based, fully implicit thermal simulator for complex reservoir processes, SPE J. 14 (2) (2009) 355–361.
[18] R. Okuno, Z. Xu, Efficient displacement of heavy oil by use of three hydrocarbon phases, SPE J. (2014), http://dx.doi.org/10.2118/165470-PA (in press).
[19] A. Iranshahr, D.V. Voskov, H.A. Tchelepi, Tie-simplex parameterization for EOS-based thermal compositional simulation, SPE J. 15 (2) (2010) 545–556.
[20] D.E.A. Van Odyck, J.B. Bell, F. Monmont, N. Nikiforakis, The mathematical structure of multiphase thermal models of flow in porous media, Proc. R. Soc. A: Math. Phys. Eng. Sci. 465 (2102) (2009) 523–549.
[21] M.L. Michelsen, Multiphase isenthalpic and isentropic flash algorithms, Fluid Phase Equilib. 33 (1–2) (1987) 13–27.
[22] M.L. Michelsen, State function based flash specifications, Fluid Phase Equilib. 158–160 (1999) 617–626.
[23] M.L. Michelsen, Phase equilibrium calculations. What is easy and what is difficult? Comput. Chem. Eng. 17 (5–6) (1993) 431–439.
[24] R.K. Agarwal, Y.K. Li, L.X. Nghiem, D.A. Coombe, Multiphase multicomponent isenthalpic flash calculations, J. Can. Pet. Technol. 30 (3) (1991) 69–75.
[25] R.K. Mehra, R.A. Heidemann, K. Aziz, Computation of multiphase equilibrium for compositional simulation, SPE J. 22 (1) (1982) 61–68.
[26] L.X. Nghiem, K. Aziz, Y.K. Li, A robust iterative method for flash calculations using the Soave–Redlich–Kwong or the Peng–Robinson equation of state, SPE J. 23 (3) (1983) 521–530.
[27] M.L. Michelsen, The isothermal flash problem. Part II. Phase-split calculation, Fluid Phase Equilib. 9 (1) (1982) 21–40.
[28] M.N. Ammar, H. Renon, The isothermal flash problem: new methods for phase split calculations, AIChE J. 33 (6) (1987) 926–939.
[29] H. Pan, A. Firoozabadi, Fast and robust algorithm for compositional modeling: part II. Two-phase flash computations, SPE J. 8 (4) (2003) 380–391.
[30] Y.-B. Chang, Development and Application of an Equation of State Compositional Simulator (PhD dissertation), The University of Texas at Austin, Austin, TX, 1990.
[31] Y.-B. Chang, G.A. Pope, K. Sepehrnoori, A higher-order finite-difference compositional simulator, J. Pet. Sci. Eng. 5 (1) (1990) 35–50.
[32] D.R. Perschke, Equation of State Phase Behavior Modeling for Compositional Simulation (PhD dissertation), The University of Texas at Austin, Austin, TX, 1988.
[33] D.R. Perschke, Y.-B. Chang, G.A. Pope, K. Sepehrnoori, Comparison of Phase Behavior Algorithms for an Equation-of-State Compositional Simulator. Paper SPE 19443 available from SPE, Richardson, Texas, 1989.
[34] M.L. Michelsen, Speeding up the two-phase PT-flash, with applications for calculation of miscible displacement, Fluid Phase Equilib. 143 (1–2) (1998) 1–12.
[35] M.L. Michelsen, J.M. Mollerup, Thermodynamic Models: Fundamentals and Computational Aspects, Tie-Line Publications, Denmark, 2004.
[36] H.H. Rachford Jr., J.D. Rice, Procedure for use of electronic digital computers in calculating flash vaporization hydrocarbon equilibrium, AIME Pet. Trans. 195 (1952) 327–328.
[37] L.X. Nghiem, A New Approach to Quasi-Newton Methods with Application to Compositional Modeling. Paper presented at the SPE Reservoir Simulation Symposium, November 15–18, San Francisco, California, 1983.
[38] L.X. Nghiem, Y.K. Li, Computation of multiphase equilibrium phenomena with an equation of state, Fluid Phase Equilib. 17 (1) (1984) 77–95.
[39] A.L. Siu, B.J. Rozon, Y.K. Li, L.X. Nghiem, W.H. Acteson, M.E. McCormack, A fully implicit thermal wellbore model for multicomponent fluid flows, SPE Reserv. Eng. 6 (3) (1991) 302–310.
[40] R.M. Enick, G.D. Holder, J.A. Grenko, A.J. Brainard, Four-phase Flash Equilibrium Calculations for Multicomponent Systems Containing Water, Equation of States: Theories and Applications. ACS Symposium Series, vol. 300, 1986.
[41] R.M. Enick, G.D. Holder, R. Mohamed, Four-phase flash equilibrium calculations using the Peng–Robinson equation of state and a mixing rule for asymmetric systems, SPE Reserv. Eng. 2 (4) (1987) 687–694.
[42] G.M.N. Costa, S. Kislansky, L.C. Oliveira, F.L.P. Pessoa, S.A.B. Vieira de Melo, M. Embiruçu, Modeling of solid–liquid equilibria for polyethylene and polypropylene solutions with equations of state, J. Appl. Polym. Sci. 121 (3) (2011) 1832–1849.
[43] R. Risnes, Equilibrium calculations for coexisting liquid phases, SPE J. 24 (1) (1984) 87–96.
[44] C.L. Yaws, X. Pan, X. Lin, Water solubility data for 151 hydrocarbons, Chem. Eng. 100 (2) (1993) 108–111.
[45] B. Amirijafari, J.M. Campbell, Solubility of gaseous hydrocarbon mixtures in water, SPE J. 12 (1) (1972) 21–27.
[46] S. Luo, M.A. Barrufet, Reservoir simulation study of water-in-oil solubility effect on oil recovery in steam injection process, SPE Reserv. Eval. Eng. 8 (6) (2005) 528–533.
[47] R. Okuno, Modeling of Multiphase Behavior for Gas Flooding Simulation (PhD dissertation), The University of Texas at Austin, Austin, TX, 2009.
[48] A. Kumar, R. Okuno, Characterization of reservoir fluids using an EOS based on perturbation from n-alkanes, Fluid Phase Equilib. 358 (2013) 250–271.
[49] D.-Y. Peng, D.B. Robinson, A new two-constant equation of state, Ind. Eng. Chem. Fundam. 15 (1) (1976) 59–64.
[50] D.-Y. Peng, D.B. Robinson, Two and three phase equilibrium calculations for systems containing water, Can. J. Chem. Eng. 54 (6) (1976) 595–599.
[51] J.D. van der Waals, On the Continuity of the Gaseous and Liquid States, 1873. Edited and With an Introduction by J.S. Rowlinson, Dover Publications, Inc., New York, 1988.
[52] R. Okuno, R.T. Johns, K. Sepehrnoori, A new algorithm for Rachford–Rice for multiphase compositional simulation, SPE J. 15 (2) (2010) 313–325.
[53] G. Wilson, A Modified Redlich-Kwong Equation of State, Application to General Physical Data Calculations. Paper presented at AIChE National Meeting, May 4–7, Cleveland, Ohio, 1969.
[54] K.A. Evelein, R.G. Moore, R.A. Heidemann, Correlation of the phase behavior in the systems hydrogen sulfide–water and carbon dioxide–water, Ind. Eng. Chem. Process Des. Dev. 15 (3) (1976) 423–428.
[55] J.W. Tester, M. Modell, Thermodynamics and Its Applications, third ed., Prentice Hall, New Jersey, 1996.
[56] B.E. Poling, J.M. Prausnitz, J.P. O'Connell, The Properties of Gases and Liquids, fifth ed., McGraw-Hill Professional, New York, 2000.
[57] N.J. Higham, Accuracy and Stability of Numerical Algorithms, second ed., SIAM, Philadelphia, PA, 2002.
[58] M. Castier, Solution of the isochoric–isoenergetic flash problem by direct entropy maximization, Fluid Phase Equilib. 276 (1) (2009) 7–17.
[59] G.H. Golub, C.F. van Van Loan, Matrix Computations, third ed., Johns Hopkins University Press, Baltimore, MD, 1996.
[60] J.E. Dennis Jr., R.B. Schnabel, Numerical Methods for Unconstrained Optimization and Nonlinear Equations, SIAM, Philadelphia, PA, 1996.
[61] D.J. Bates, J.D. Hauenstein, A.J. Sommese, C.W. Wampler, Numerically Solving Polynomial Systems with Bertini (Software, Environments and Tools), vol. 25, SIAM, Philadelphia, PA, 2013.
[62] V. Chatoorgoon, SPORTS – a simple non-linear thermal hydraulic stability code, Nucl. Eng. Des. 93 (1) (1986) 51–67.
[63] M.L. Overton, Numerical Computing with IEEE Floating Point Arithmetic, first ed., SIAM, Philadelphia, PA, 2001.